Supporting Information

Exploiting Singlet Fission in *para*-Azaquinodimethane Nanoaggregates with High Energy Triplets to Trigger Phototoxic Reactive Oxygen Species

Experimental Section

Nanoaggregate preparation. The investigated molecules were synthesized according to the procedure detailed in a previous study.[1] Nanoaggregates in water dispersion were prepared by injection in water of a concentrated (about 1 mM) organic solution (DMSO or THF) of the investigated compounds, with a ratio of 1:100 (v:v, organic solution:water), and mixed by sonication.[2,3] Samples for fluorimetric experiments for ROS detection were prepared by using a probe sonicator (VIRTIS Virsonic 60, Steroglass) at 10 W power for 3 minutes to assist the formation of well-dispersed nanoaggregates.

Photophysical experiments. Spectral and photophysical properties were recorded in Dimethylsulphoxide (DMSO) and water. Stationary absorption measurements were carried out by a Varian Cary 1 UV-Visible spectrophotometer. An FS5 Spectrofluorimeter by Edinburgh Instruments, operated by Fluoracle software, was used for excitation/emission fluorescence for the samples in solution as well as in water dispersion. Air-equilibrated dilute solutions (absorbance < 0.1 at the excitation wavelength) were used for the fluorimetric measurements. The fluorescence quantum yields (Φ_F, experimental error ± 10%) were obtained by employing tetracene (Φ_F = 0.17 in air-equilibrated cyclohexane) and Rhodamine 6G (Φ_F = 0.95 in air-equilibrated ethanol) as reference compounds,[4] taking also into account the different refractive indexes of the used solvents. Fluorescence lifetimes were measured through an Edinburgh Instrument 199S Spectrofluorimeter equipped with the single photon counting technique. Several LEDs centered at 370, 450, and 510 nm were used as light sources (temporal resolution = 0.5 ns).
Triplet properties were measured by laser flash photolysis (Edinburgh LP980) upon excitation at 355 nm (third harmonic of a Quanta-Ray/ INDI Nd:YAG laser, Spectra Physics) with nanosecond time resolution (pulse width 7 ns and laser energy < 1 mJ per pulse) coupled with a PMT for signal detection. The excitation at 355 nm was the pump-pulse while a pulsed xenon lamp was used to probe the absorption properties of the produced excited states. The experimental setup was calibrated by an optically matched solution of benzophenone (Bz) in MeCN (Φ_T = 1 and ε_T = 6500 M^{-1} cm^{-1} at 520 nm).[5] Triplet–triplet absorption coefficients (ε_T) were evaluated by energy transfer experiment from benzophenone to the studied compounds in MeCN. The triplet quantum yields, Φ_T, were determined (estimated uncertainty of ±15%) by an actinometry approach considering Bz in MeCN as the reference. All measurements were performed by purging the sample with pure molecular nitrogen. The detailed methodologies concerning the determination of the triplet extinction coefficient and quantum yield have been extensively discussed in the Supporting Information of a previous work published by our research group.[6]
The experimental setup for ultrafast transient absorption experiments has been previously reported.[7] The 400 nm excitation pulses (ca. 60 fs) were generated as the second harmonic of an amplified Ti:Sapphire laser system (Spectra Physics). The 500 nm excitation pulses were obtained through the use of TOPAS Prime and its NIR-UV harmonic generator (Spectra Physics), triggered by the output of the amplified Ti:Sapphire laser system (Spectra Physics). The Helios transient absorption spectrometer (Ultrafast Systems) is characterized by a temporal resolution of about 150 fs and a spectral resolution of 1.5 nm. A small portion of the 800 nm light passes through an optical delay line (time window of 3200 ps) and is focused onto a Sapphire crystal (2 mm thick) to generate a white-light in the 450-800 nm spectral range (probe pulse). All measurements were carried out under the magic angle relative polarization condition in 2 mm cuvettes at an absorbance of about 0.5 at 400 nm. The solution was stirred during the experiments to avoid photoproduct interferences. Photodegradation was checked by recording the absorption spectra before and after the time-resolved measurements, where no significant change was observed. The experimental 3D data matrices were firstly analyzed by performing the Global Analysis by Surface Xplorer PRO (Ultrafast Systems) software, and successively through GloTarAn software in order to obtain the Evolution-Associated Spectra (EAS) considering a consecutive kinetic model. The uncertainty estimated on the lifetimes derived through this multiexponential fitting procedure is of ca. 10%.
Two−photon excited fluorescence measurements were performed using an amplified mode−locked Ti:Sapphire laser system (Spectra Physics) at 800 nm delivering ca. 60 fs output pulses at 1 kHz repetition rate. Input power from the laser was varied using a variable neutral density filter. The excitation laser beam was focused on the sample solutions using an iris. The 1 cm quartz cuvette

containing the solution was placed on the sample holder so as to have the fluorescence generated on the close vicinity of the wall of the cuvette to limit reabsorption of fluorescence. The fluorescence was then collected in epifluorescence through an optical fiber coupled to a CCD detector (BWTEK BRC111A). Emission spectra were obtained under the 800-nm excitation by using the CCD detector. The two−photon excited fluorescence emission spectra were analyzed to determine the two−photon absorption cross−section through the comparative method according to the following equation:

$$\delta_{sample} = \delta_{reference} \times \frac{Area_{F,sample}}{Area_{F,reference}} \times \frac{\phi_{F,reference}}{\phi_{F,sample}} \times \frac{c_{reference}}{c_{sample}}$$

where δ is the two-photon absorption cross-section at the excitation wavelength, $Area_F$ is the integral of the recorded emission spectrum, ϕ_F is the fluorescence quantum yield and c is the solution concentration. The accuracy of this set up in determining the two-photon absorption cross sections was calibrated by using two well−known two-photon absorbing and highly fluorescent reference compounds: rhodamine B in ethanol (cross−section 120 GM at 800 nm) and fluorescein in buffered water at pH 11 (cross−section 26 GM at 800 nm).[3,8] Rhodamine B in ethanol was used as the reference compound for the samples here investigated.

The morphology of the water-dispersed nanoaggregates was analyzed by a field emission scanning electron microscope (FE-SEM), a GeminiSEM 360 (ZEISS). Each sample was deposited on a circular Si slice (12 mm in diameter and 1 mm thick) and dried at room temperature. Before the analysis, the samples were attached to an aluminum support using conductive carbon adhesive tape. Measurements were carried out using an In-lens detector at 1kV.

Hydrodynamic diameters of the nanoaggregates were evaluated using the Dynamic Light Scattering technique, in particular with a Nicomp NanoDLS/ZLS instrument, which measures size and potential of sub-micron particles using a red laser diode (630nm) and two detectors, APD for particle size and PMT for zeta potential.

ROS production under irradiation was evaluated for the nanoaggregates in water dispersion by using two specific probes, SOSG (Singlet Oxygen Sensor Green) for the detection of $^1O_2$ and DHE (Dihydroethidium) for the detection of the superoxide anion.[9,10] For the SOSG experiment: 2 mL of probe-sonicated nanoaggregates were put in the cuvette together with 25 µL of SOSG (stock solution 0.5mM in MeOH) to obtain a final concentration of 6.2 µM inside the cuvette. Samples were then exposed to 458 nm LED irradiation at a power density of 1.07mW/cm². Fluorescence was monitored before irradiation and after increasing irradiation times with an Edinburgh Instruments FS5 spectrofluorometer by exciting the samples at 488 nm. Control experiments were performed with SOSG alone to evaluate the effect of light on the fluorescence of the probe. Ratios of the areas subtended by the emission spectra recorded at increasing irradiation times over the area of the initial emission spectra of SOSG were then plotted as a function of irradiation times and fitted with a linear regression function to obtain the slope, as an indicator of $^1O_2$ production efficiency. Similarly, for the DHE experiment: 2 mL of probe-sonicated nanoaggregates were put in the cuvette together with 4 µL of DHE (stock solution 10mM in DMSO) to obtain a concentration of 20 µM inside the cuvette. Samples were then exposed to 458 nm LED irradiation at a power density of 1.07 mW/cm². Fluorescence was monitored before irradiation and after increasing irradiation times with an Edinburgh Instruments FS5 spectrofluorometer by exciting the samples at 480 nm. Control experiments were performed with DHE alone to evaluate the effect of light on the fluorescence of the probe. Ratios of the areas subtended by the emission spectra recorded at increasing irradiation times over the area of the initial emission spectra of DHE were then plotted as a function of irradiation times to evaluate the superoxide anion production efficiency.

Biological Experiments.

Materials

Dulbecco's modified Eagle's medium (DMEM), Roswell Park Memorial Institute (RPMI), fetal bovine serum (FBS), Trypsin, and Penicillin/Streptomycin were purchased from Euroclone. Dimethyl sulfoxide (DMSO), Trypan Blue powder, 2',7'-Dichlorodihydrofluorescein Diacetate (DCFH-DA), and 3-(4,5-dimethylthiazol-2-yl)-2,5-diphenyltetrazolium bromide (MTT), and VECTASHIELD Vibrance® Antifade Mounting Medium containing DAPI were purchased from Sigma-Aldrich and from Becton, Dickinson and Company.

SK-MEL-5 and LN-CaP Cell Culture

SK-MEL-5 (MEL-501) human melanoma cells and LN-CaP human prostate cancer cells were purchased from ATCC (Manassas, VA, USA). Cells were cultured in DMEM and RPMI medium, respectively, containing 10% (v/v) heat-inactivated FBS, Penicillin 10,000 U/mL, and Streptomycin 10 mg/mL. The cell concentration was monitored by Trypan blue dye staining using an automated cell counter (Invitrogen™ Countess™, Thermo Fisher Scientific, Waltham, MA, USA).

Cytotoxicity and phototoxicity MTT assay

The effect of the water-dispersed nanoaggregates of the four para-azaquinodimethane (pAQM) compounds on cell proliferation was studied by the MTT assay both in the dark and after photoirradiation. 2,000 SK-MEL-5 and LN-CaP cells were seeded in Falcon® 96-well clear flat-bottom microplates with 200 µL of DMEM or RPMI medium, respectively, and after 24 hours of incubation, different aliquots of the compounds' stock solution (10^{-3} M in DMSO) diluted in the medium were added to each well to reach concentrations ranging from 10 to 0.01 µM in octuplicate. Two quadruplets were kept as vehicle controls to take into account the contribution of the DMSO used. To test the phototoxicity, cells were then photoexposed in an LED chamber at a power density of

1.07 mW/cm² for 28 minutes. After 72 hours of incubation in a humidified atmosphere with 5% CO_2 at 37 °C, 20 µL of a 5 mg/mL MTT dye solution were added to each well to reach a final concentration of 0.5 mg/mL. The cells were then incubated in a humidified atmosphere with 5% CO_2 at 37 °C for 3 hours to allow the formation of formazan, which was subsequently dissolved in 150 µL of DMSO at 37 °C for 1 hour. After a brief mechanical shaking of the microplates, absorbance was measured at 570 nm using a Tecan Infinite® spectrophotometer. Cell viability was then obtained by dividing the mean absorbance value for each concentration by the average absorbance of the vehicle controls and expressed as percentages. Measurements were performed in three independent experiments.

Intracellular ROS production

Intracellular reactive oxygen species (ROS) levels were assessed using the DCFH2-DA assay.[11]10,000 SK-MEL-5 and LN-CaP cells were seeded into each well of a black, round-bottom 96-well microplate (Corning Incorporated, Corning, NY) in 200 µL of DMEM or RPMI culture medium, respectively. The following day, the medium was replaced with fresh medium containing the water-dispersed nanoaggregates of the four pAQM compounds at the same concentrations used for the cytotoxicity assay. A set of four wells was used as vehicle control to assess the effect of DMSO. Cells were then photoexposed in an LED chamber at a power density of 1.07 mW/cm² for 28 minutes. After 24 hours, cells were washed with 100 µL of PBS and incubated with 10 µM DCFH2-DA (stock solution 0.02 M in DMSO) for 60 minutes in a humidified atmosphere at 37 °C and 5% CO_2. Subsequently, wells were washed again with 100 µL of PBS and filled with 200 µL of fresh PBS. The fluorescence intensity of oxidized DCF was measured using a Tecan Infinite® spectrofluorimeter at excitation/emission wavelengths of 485/530 nm. Data were expressed as the percentage of fluorescence intensity relative to vehicle control and normalized to cell viability, which was assessed via the MTT assay on parallel cultures seeded and treated under the same experimental conditions, using clear 96-well microplates (Falcon, Becton, Dickinson and Company, Franklin Lakes, NJ). Measurements were performed in three independent experiments.

Fluorescence Microscopy

SK-MEL-5 (MEL-501) and LN-CaP cells were seeded on round glass coverslips previously sterilized by 30-second immersion in 70% ethanol, rinsed with sterile phosphate buffer saline (PBS), and placed in a Falcon® 24-well clear flat-bottom multiwell cell culture plate. The cells were then incubated for 45 minutes in a humidified atmosphere with 5% CO_2 at 37 °C, at the end of which 500 µL of DMEM or RPMI medium, respectively, were gently added to each well. After that, cells were incubated for 24 hours under canonical culture conditions (humidified atmosphere with 5% CO_2 at 37 °C). Then, 400 µL of water-dispersed nanoaggregates of the four pAQM compounds, diluted in DMEM and RPMI at a final concentration of 10 µM, were administered to the cells, and the multiwell was incubated for 2 hours in a humidified atmosphere with 5% CO_2 at 37 °C. Cells on round glass coverslips were then rinsed twice with PBS and fixed in 4% paraformaldehyde for 20 minutes at room temperature. The samples were then mounted, staining nuclei with VECTASHIELD Vibrance® Antifade Mounting Medium containing DAPI, and image acquisition was performed using a fluorescence microscope (Eclipse TE2000-S, Nikon) equipped with the F-View II FireWire camera and through the use of CellF Imaging Software (Olympus Soft Imaging Solutions).

Absorption and Fluorescence Properties

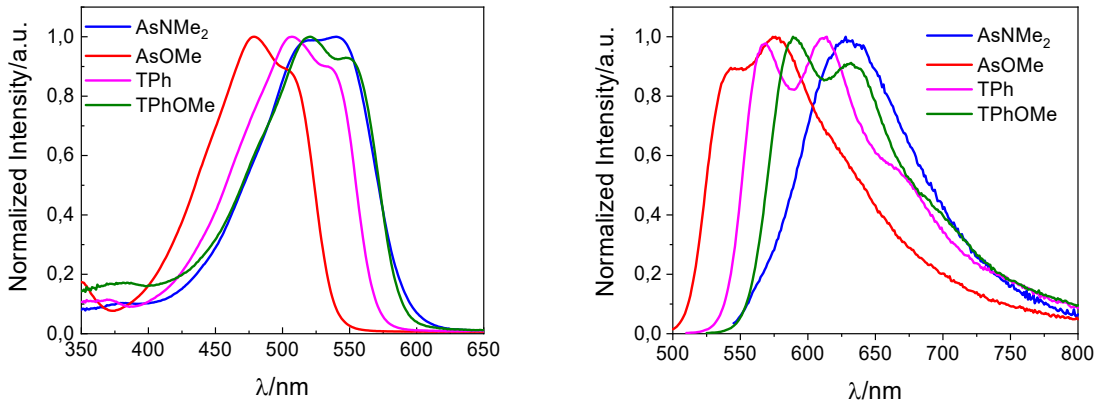

Figure S1. Normalized absorption and emission spectra of the investigated compounds in DMSO.

Table S1. Spectral and fluorescence properties of the compounds in DMSO. λ_{abs}, λ_{em}: maximum wavelengths of absorption and emission spectra; Φ_F: fluorescence quantum yield; τ_F: fluorescence lifetime; k_F: fluorescence rate constants computed as Φ_F/τ_F.

Compound	λ_{abs} / nm	λ_{em} / nm	Φ_F	τ_F / ps	k_F / 10^8 s^{-1}
AsOMe	479	575	0.066	310*	2.1
$AsNMe_2$	540	630	0.014	99*	1.4
TPh	507	610	0.156	1030	1.5
TPhOMe	521	595	0.158	770	2.0

*from fs-TA

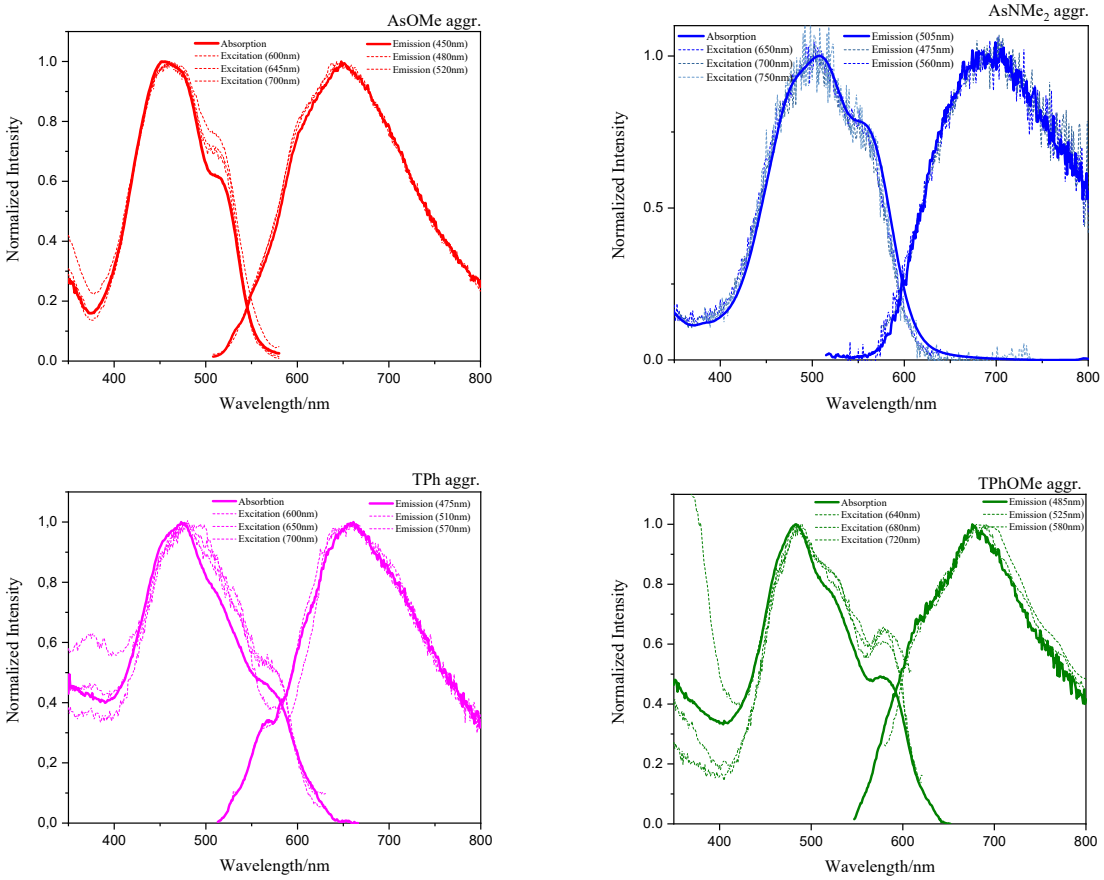

Figure S2. Normalized absorption, fluorescence emission and excitation spectra of nanoaggregates of the investigated compounds in water.

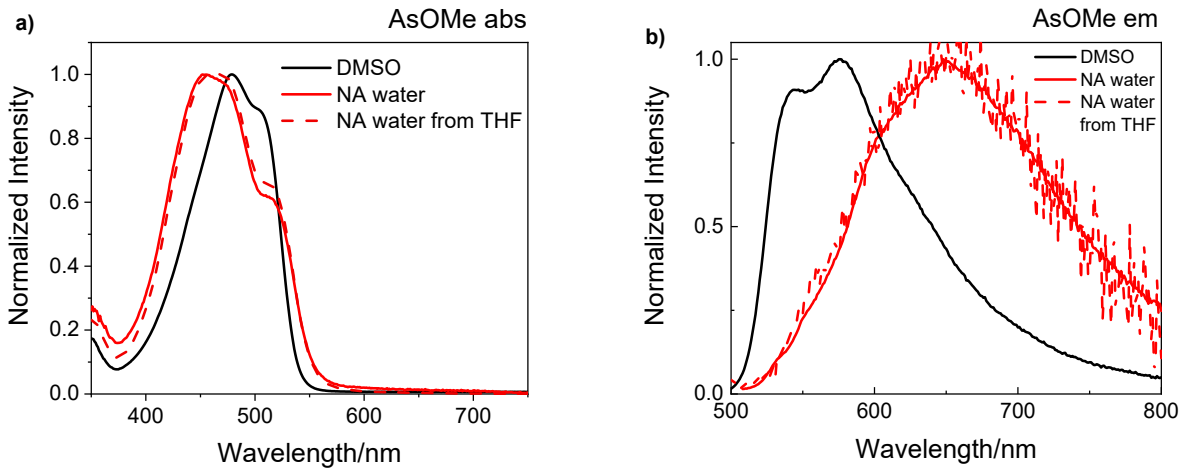

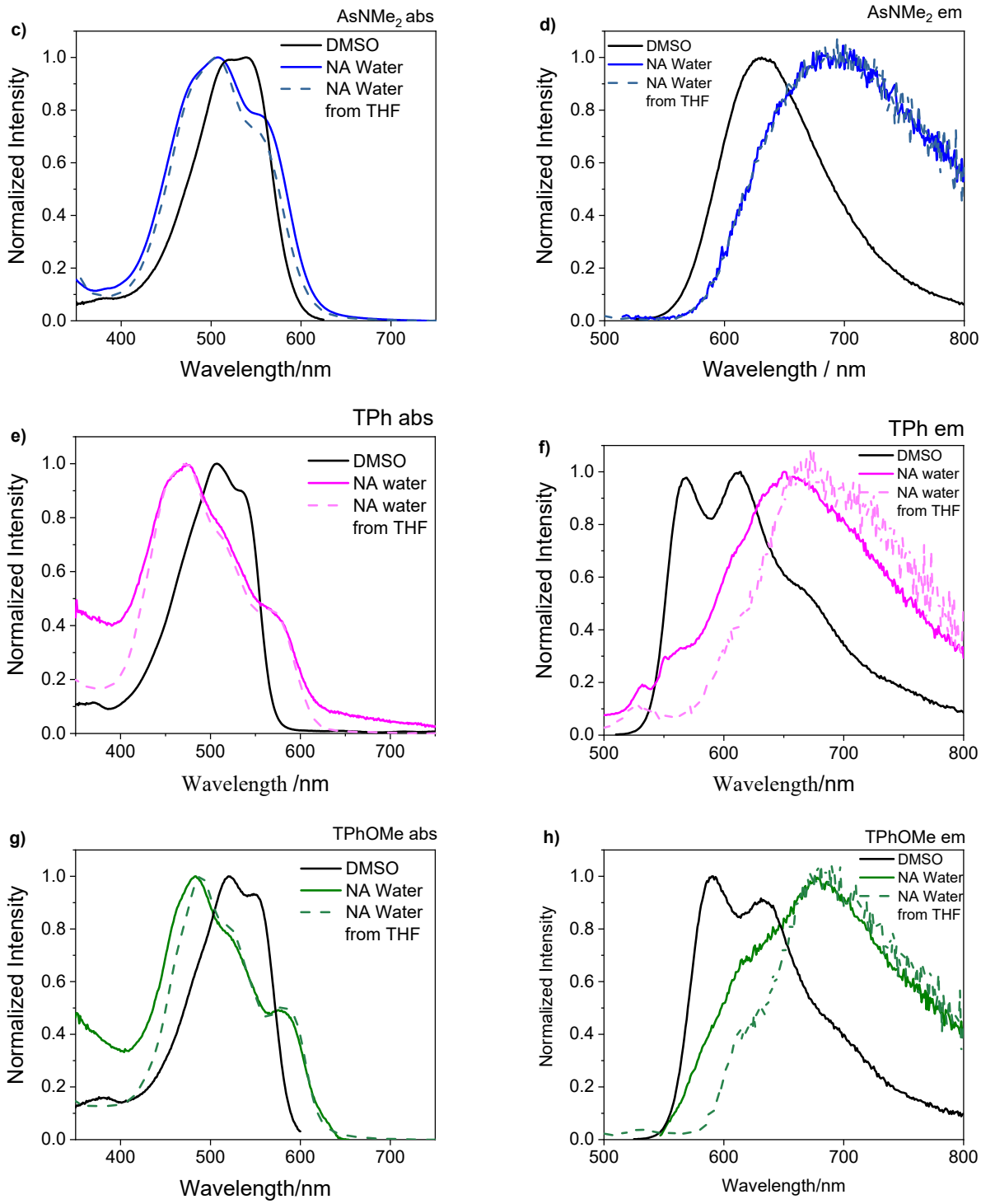

Figure S3. Comparison between absorption and emission spectra of the investigated compounds in DMSO solution (black lines) and water-dispersed nanoaggregates obtained upon injection of a concentrated DMSO (coloured solid lines) or THF (coloured dashed lines) solution.

Table S2. Absorption and emission spectral shifts passing from the monomer to the J-aggregate for all the investigated compounds.

Compound	Absorption Shift (monomer-Jaggregate) / cm^{-1}	Emission Shift (monomer-aggregate) / cm^{-1}
AsOMe	1420	2000
$AsNMe_2$	630	1440
TPh	2150	2340
TPhOMe	1990	2300

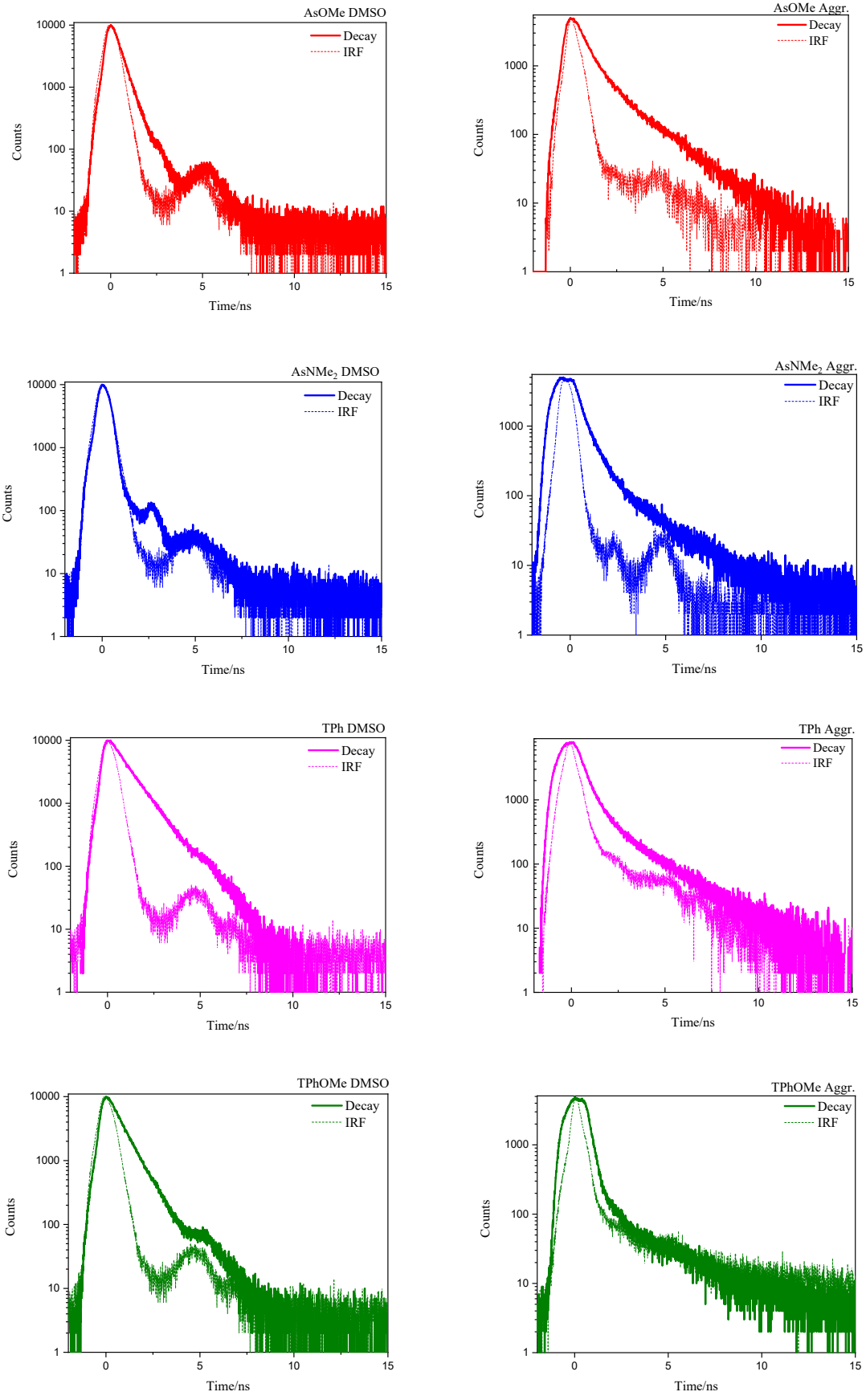

Figure S4. Fluorescence decay kinetics obtained through TC-SPC for the investigated compounds in DMSO solution (left) and water-dispersed nanoaggregates (right).

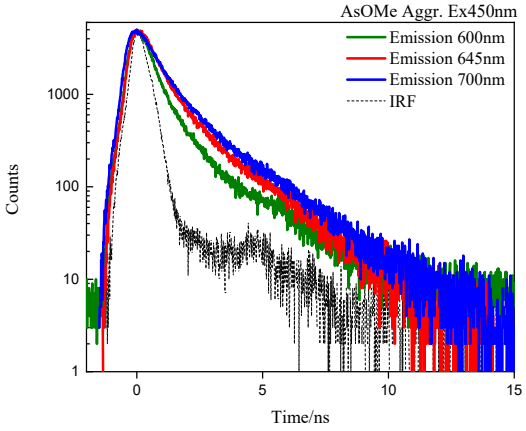
AsOMe Aggr. Ex450nm
Emission 600nm
Emission 645nm
Emission 700nm
IRF
Counts
Time/ns

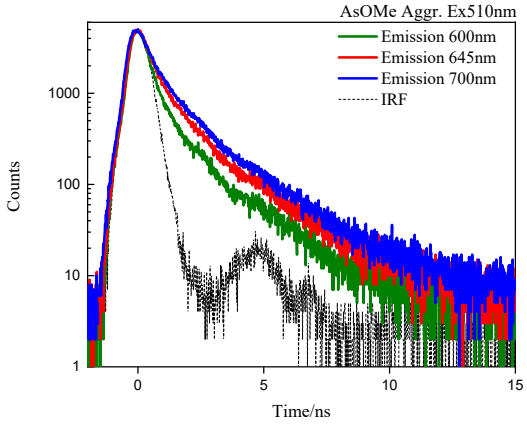
AsOMe Aggr. Ex510nm
Emission 600nm
Emission 645nm
Emission 700nm
IRF
Counts
Time/ns

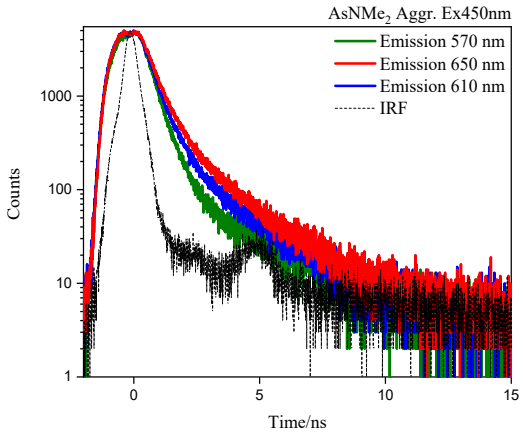
AsNMe2 Aggr. Ex450nm
Emission 570 nm
Emission 650 nm
Emission 610 nm
IRF
Counts
Time/ns

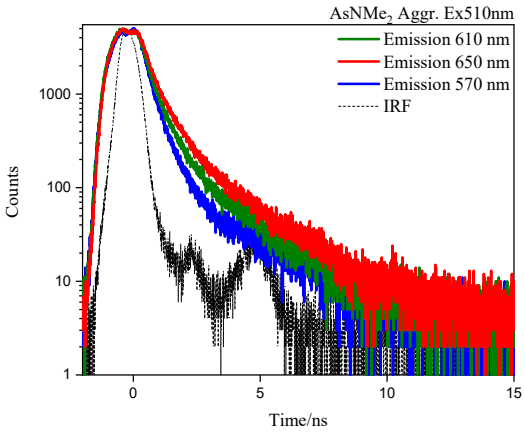
AsNMe2 Aggr. Ex510nm
Emission 610 nm
Emission 650 nm
Emission 570 nm
IRF
Counts
Time/ns

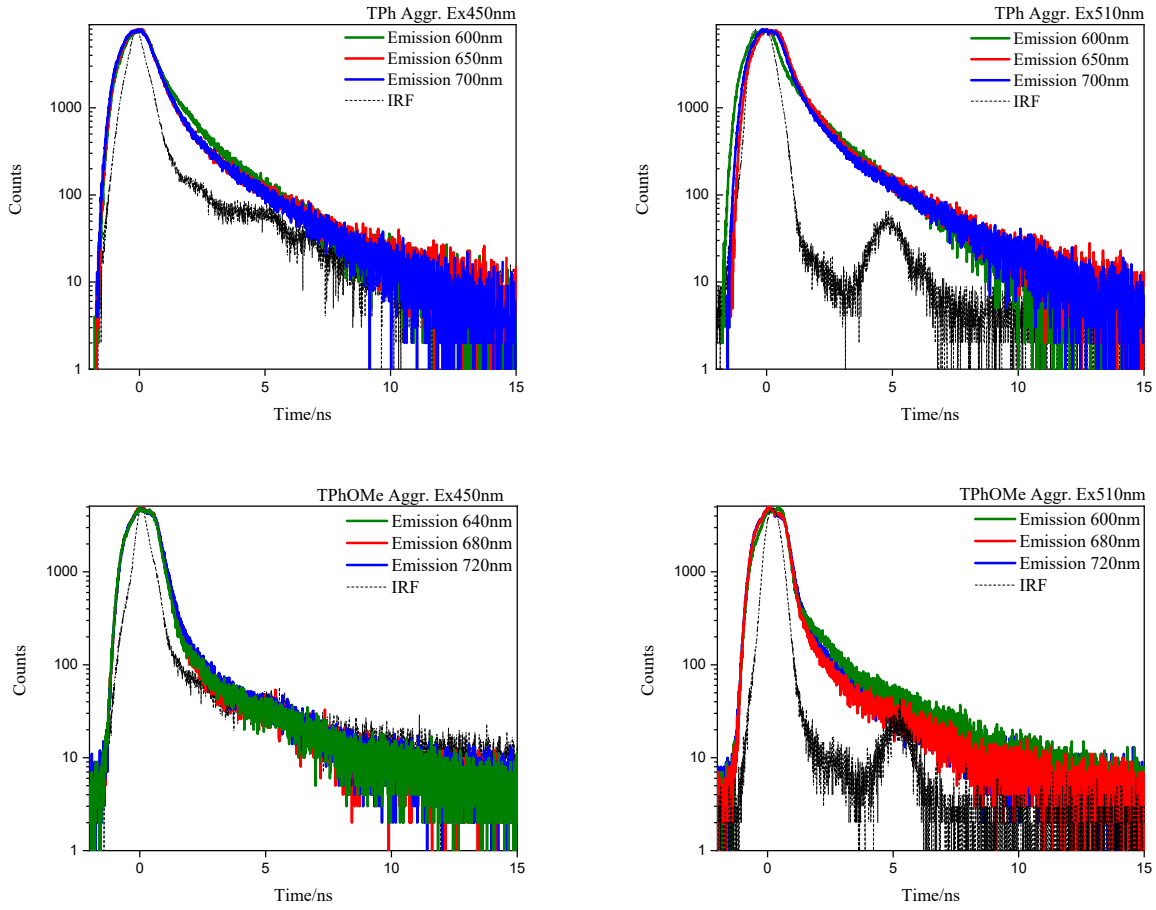

Figure S5. Wavelength effects on the fluorescence decay kinetics obtained through TC-SPC for the investigated compounds in water-dispersed nanoaggregates.

Table S3. Aggregation effect on the fluorescence lifetimes.

	τ_F /ps DMSO	τ_F /ps Aggr.
AsOMe	310*	<500 (50%) 1400 (50%)
AsNMe$_2$	99*	740
TPh	1000	590
TPhOMe	770	< 500

*from fs-TA

Nanosecond Transient Absorption

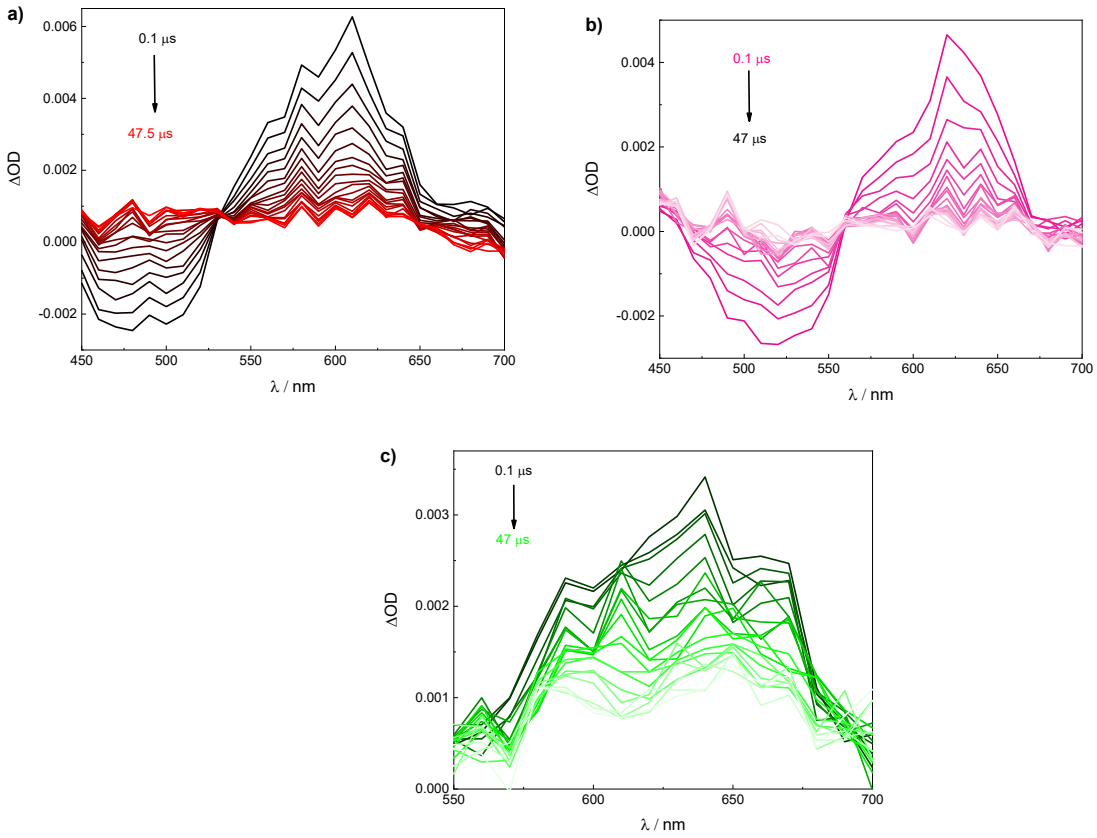

Figure S6. Nanosecond laser flash photolysis transient absorption spectra of **AsOMe** (a), **TPh** (b), and **TPhOMe** (c) in DMSO.

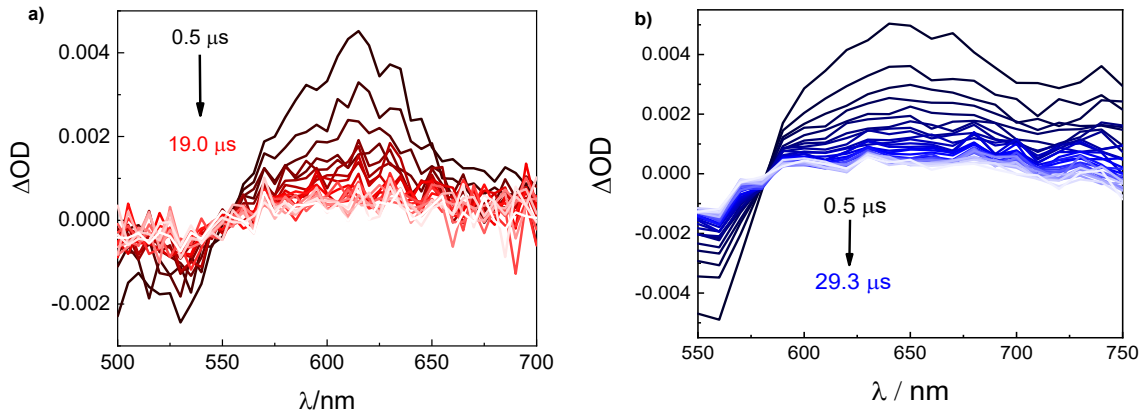

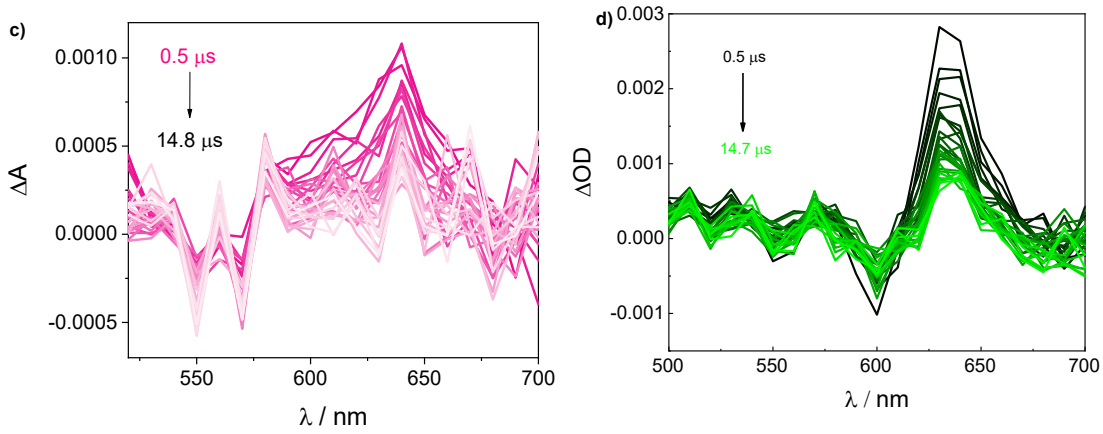

Figure S7. Nanosecond laser flash photolysis transient absorption spectra of **AsOMe** (a), **AsNMe$_2$** (b), **TPh** (c), and **TPhOMe** (d) in water-dispersed nanoaggregates.

Femtosecond Transient Absorption

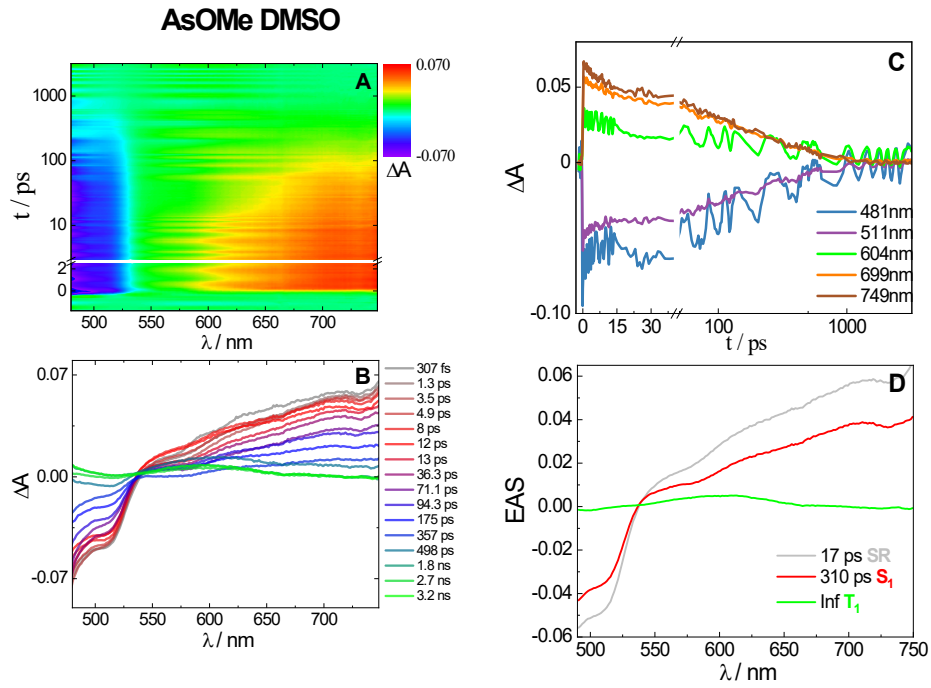

Figure S8. Femtosecond transient absorption matrix (A), spectra at different delay times (B), kinetics at different wavelengths (C), Evolution Associated Spectra (EAS) and lifetimes (D) obtained from Global Analysis for **AsOMe** in DMSO with a laser fluence of 300 μJ/cm^2.

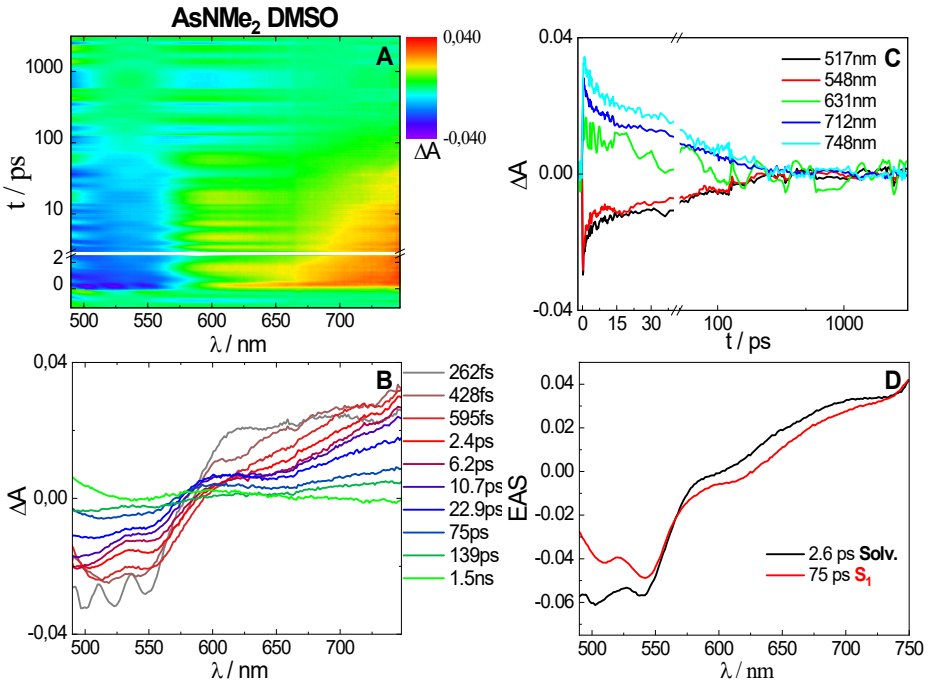

Figure S9. Femtosecond transient absorption matrix (A) spectra at different delay times (B), kinetics at different wavelengths (C), Evolution Associated Spectra (EAS) and lifetimes (D) obtained from Global Analysis for **AsNMe$_2$** in DMSO with a laser fluence of 300 μJ/cm^2.

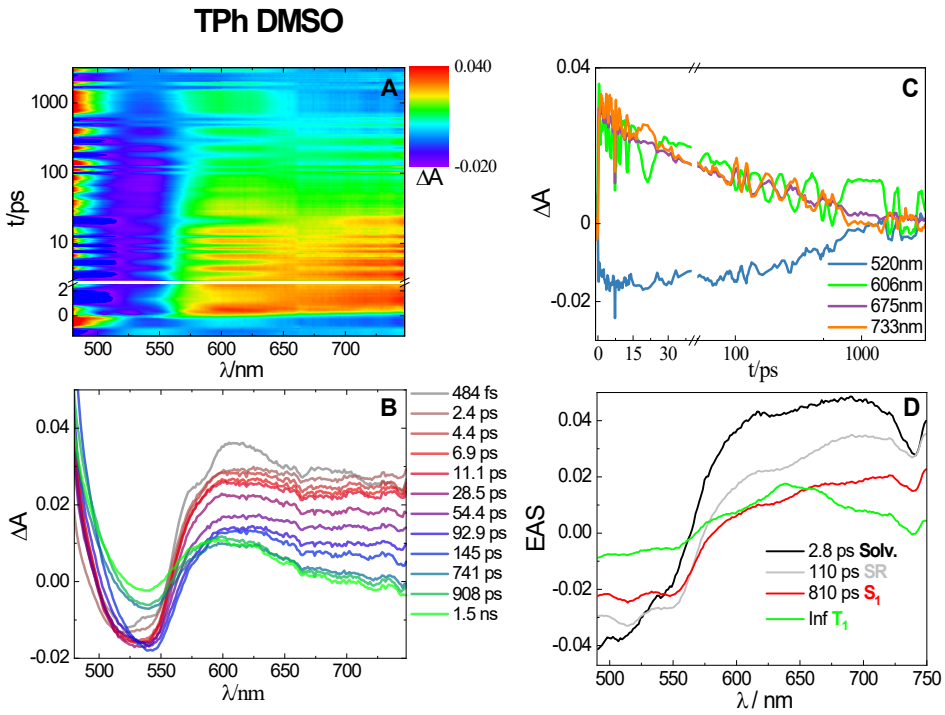

Figure S10. Femtosecond transient absorption matrix (A) spectra at different delay times (B), kinetics at different wavelengths (C), Evolution Associated Spectra (EAS) and lifetimes (D) obtained from Global Analysis for **TPh** in DMSO with a laser fluence of 300 μJ/cm^2.

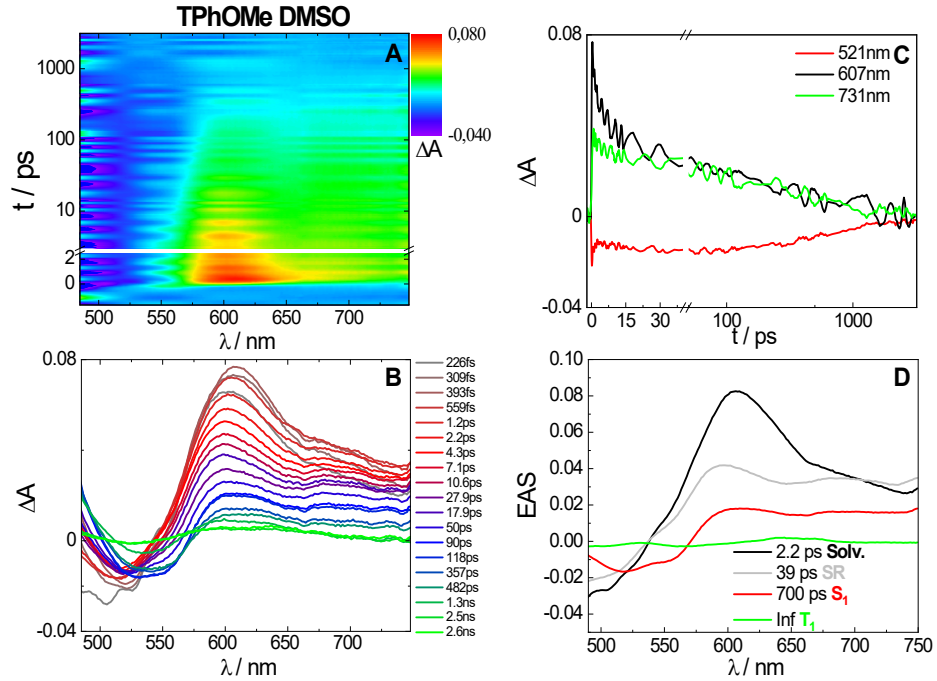

Figure S11. Femtosecond transient absorption matrix (A) spectra at different delay times (B), kinetics at different wavelengths (C), Evolution Associated Spectra (EAS) and lifetimes (D) obtained from Global Analysis for **TPhOMe** in DMSO with a laser fluence of 300 μJ/cm^2.

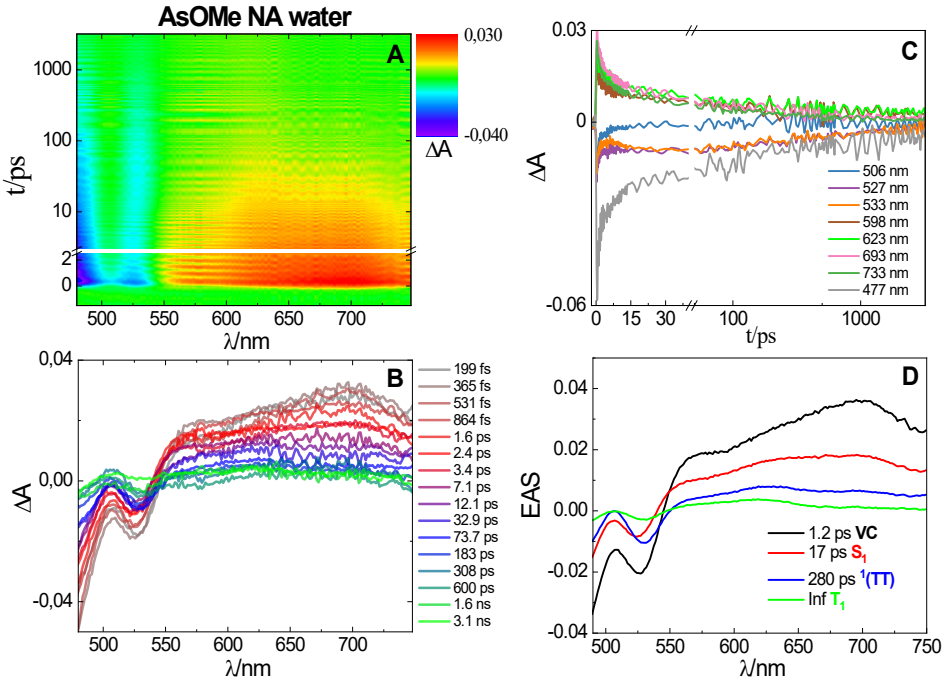

Figure S12. Femtosecond transient absorption matrix (A) spectra at different delay times (B), kinetics at different wavelengths (C), Evolution Associated Spectra (EAS) and lifetimes (D) obtained from Global Fit for **AsOMe** in water NA upon excitation at 400 nm with a laser fluence of 300 μJ/cm^2.

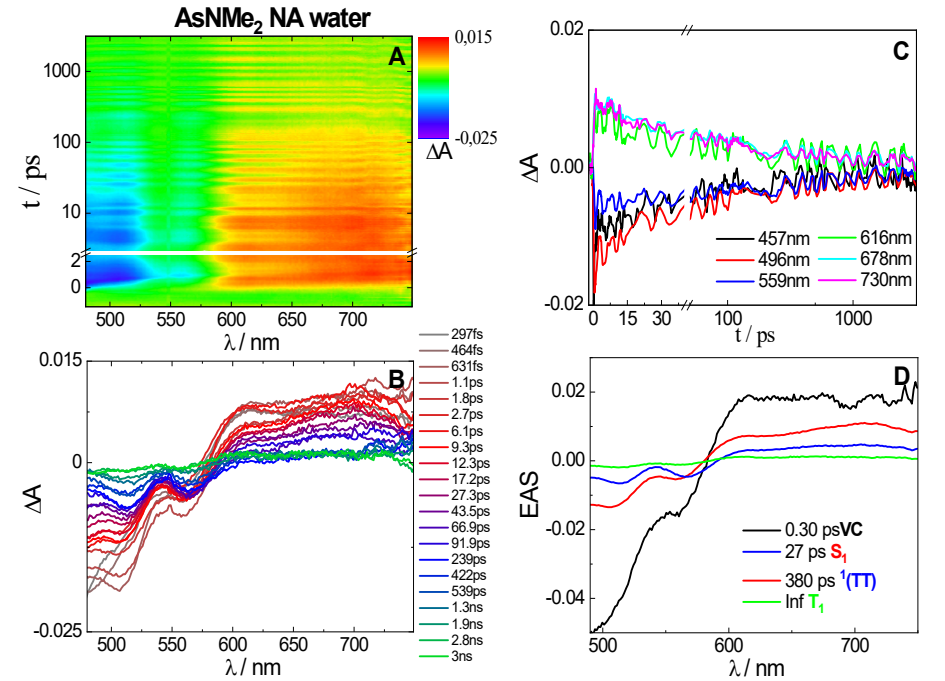

Figure S13. Femtosecond transient absorption matrix (A) spectra at different delay times (B), kinetics at different wavelengths (C), Evolution Associated Spectra (EAS) and lifetimes (D) obtained from Global Fit for **AsNMe$_2$** in water NA upon excitation at 400 nm with a laser fluence of 300 μJ/cm^2.

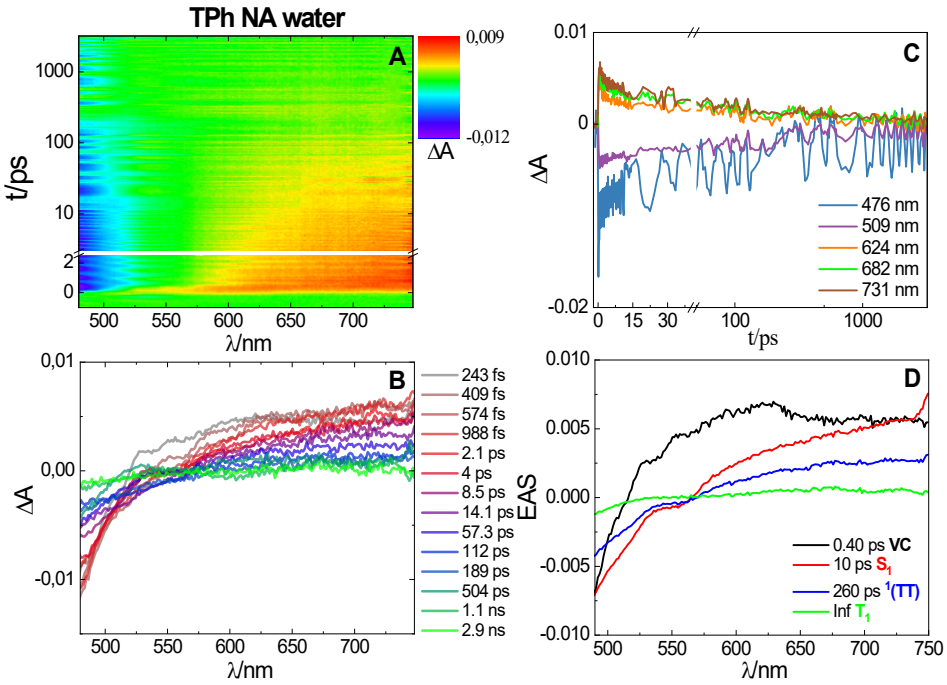

Figure S14. Femtosecond transient absorption matrix (A) spectra at different delay times (B), kinetics at different wavelengths (C), Evolution Associated Spectra (EAS) and lifetimes (D) obtained from Global Fit for **TPh** in water NA upon excitation at 400 nm with a laser fluence of 300 μJ/cm^2.

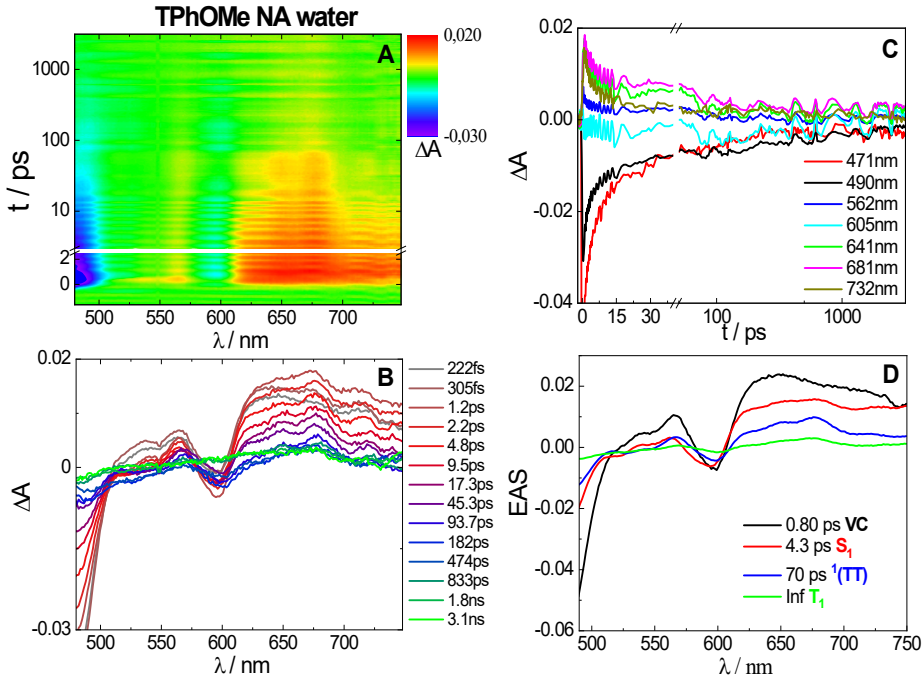

Figure S15. Femtosecond transient absorption matrix (A) spectra at different delay times (B), kinetics at different wavelengths (C), Evolution Associated Spectra (EAS) and lifetimes (D) obtained from Global Fit for **TPhOMe** in water NA upon excitation at 400 nm with a laser fluence of 300 μJ/cm^2.

Table S4. Femtosecond transient absorption results for all the investigated compounds in DMSO and water-dispersed nanoaggregates upon excitation at 400 nm with a laser fluence of 300 μJ/cm^2: lifetimes resulting from Global Analysis and relative assignment.

Compound	Environment	τ / ps	Assignment
AsOMe	DMSO	17	SR
		310	S_1
		Inf	T_1
	NA water	1.2	VC
		17	S_1
		280	^{1}(TT)
		Inf	T_1
$AsNMe_2$	DMSO	2.6	SR
		75	S_1
	NA water	0.30	VC
		27	S_1
		380	^{1}(TT)
		Inf	T_1
TPh	DMSO	2.8	Solv.
		110	SR
		810	S_1
		Inf	T_1
	NA water	0.40	VC
		10	S_1
		260	^{1}(TT)
		Inf	T_1
TPhOMe	DMSO	2.2	Solv.
		39	SR
		700	S_1
		Inf	T_1
	NA water	0.80	VC
		4.3	S_1
		70	^{1}(TT)
		Inf	T_1

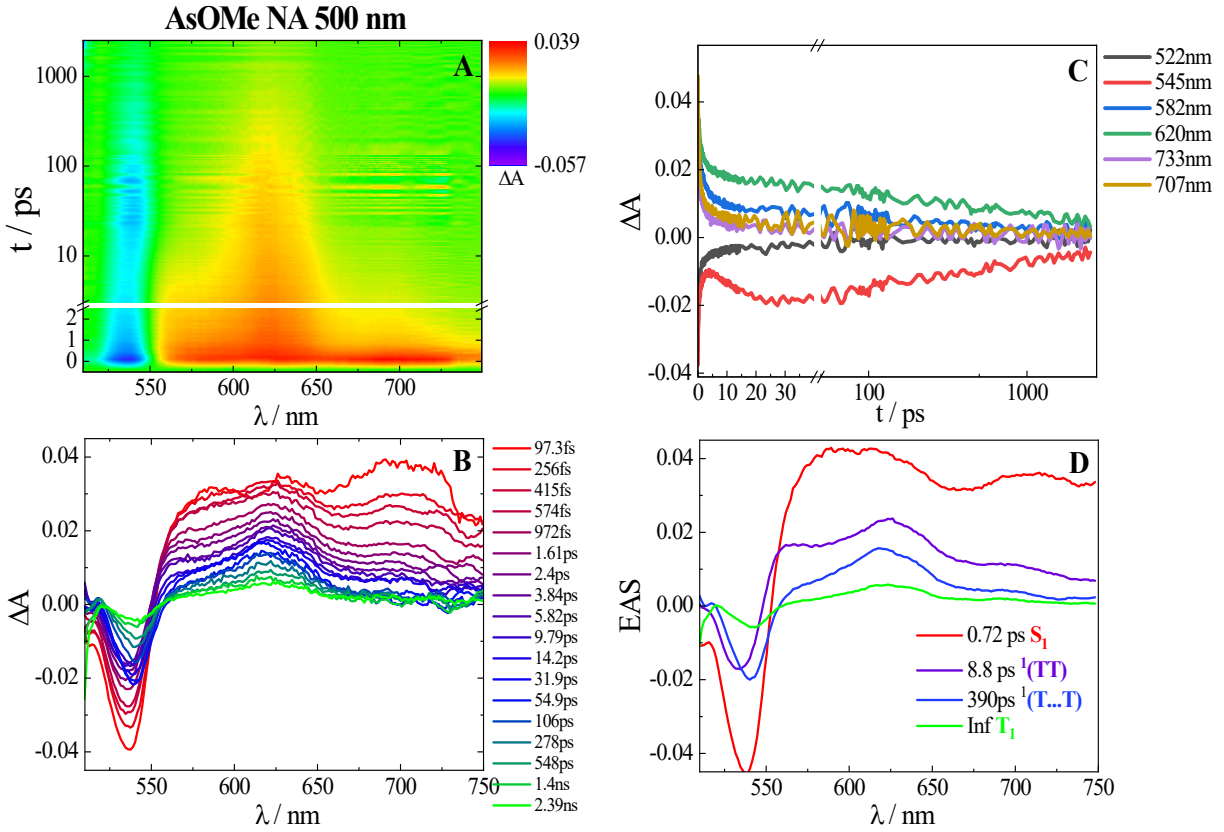

Figure S16. Femtosecond transient absorption matrix (A) spectra at different delay times (B), kinetics at different wavelengths (C), Evolution Associated Spectra (EAS) and lifetimes (D) obtained from Global Fit for **AsOMe** in water NA upon excitation at 500 nm with a laser fluence of 190 μJ/cm².

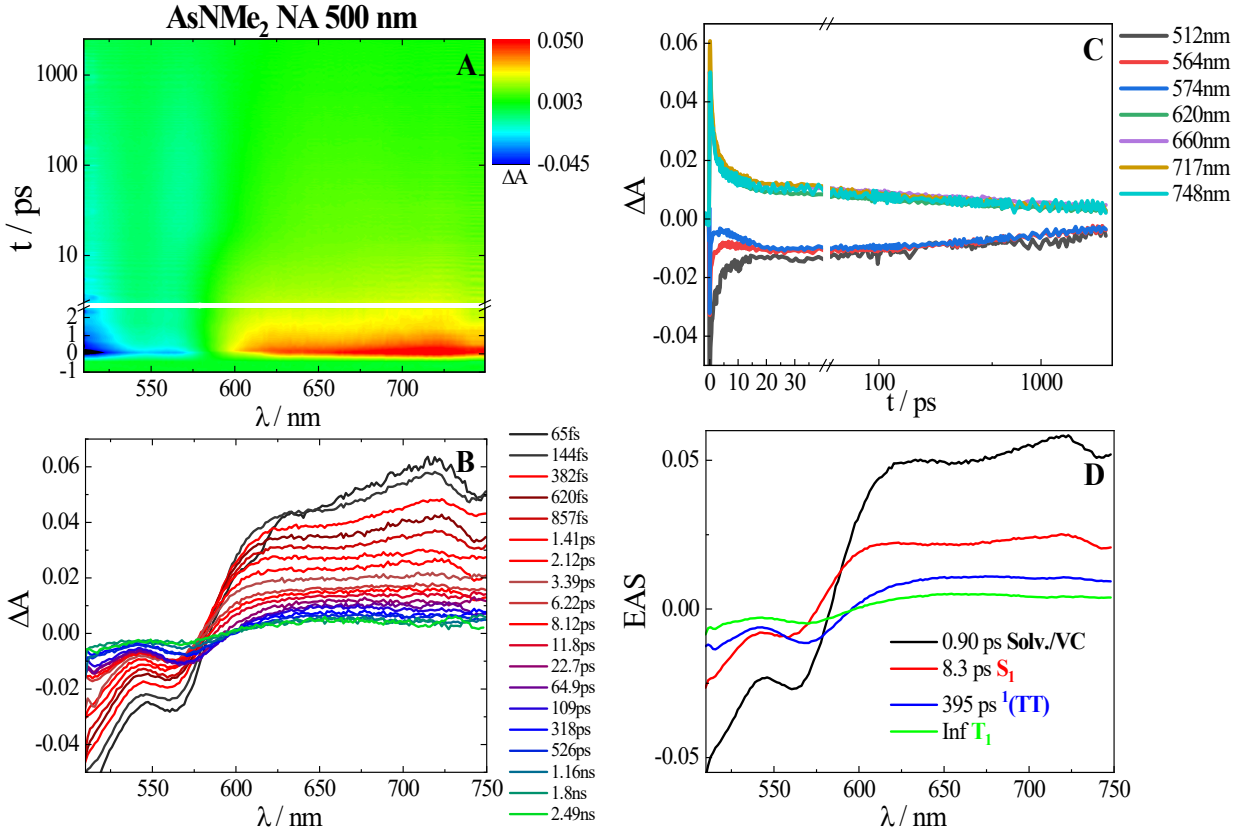

Figure S17. Femtosecond transient absorption matrix (A) spectra at different delay times (B), kinetics at different wavelengths (C), Evolution Associated Spectra (EAS) and lifetimes (D) obtained from Global Fit for **$AsNMe_2$** in water NA upon excitation at 500 nm with a laser fluence of 190 μJ/cm².

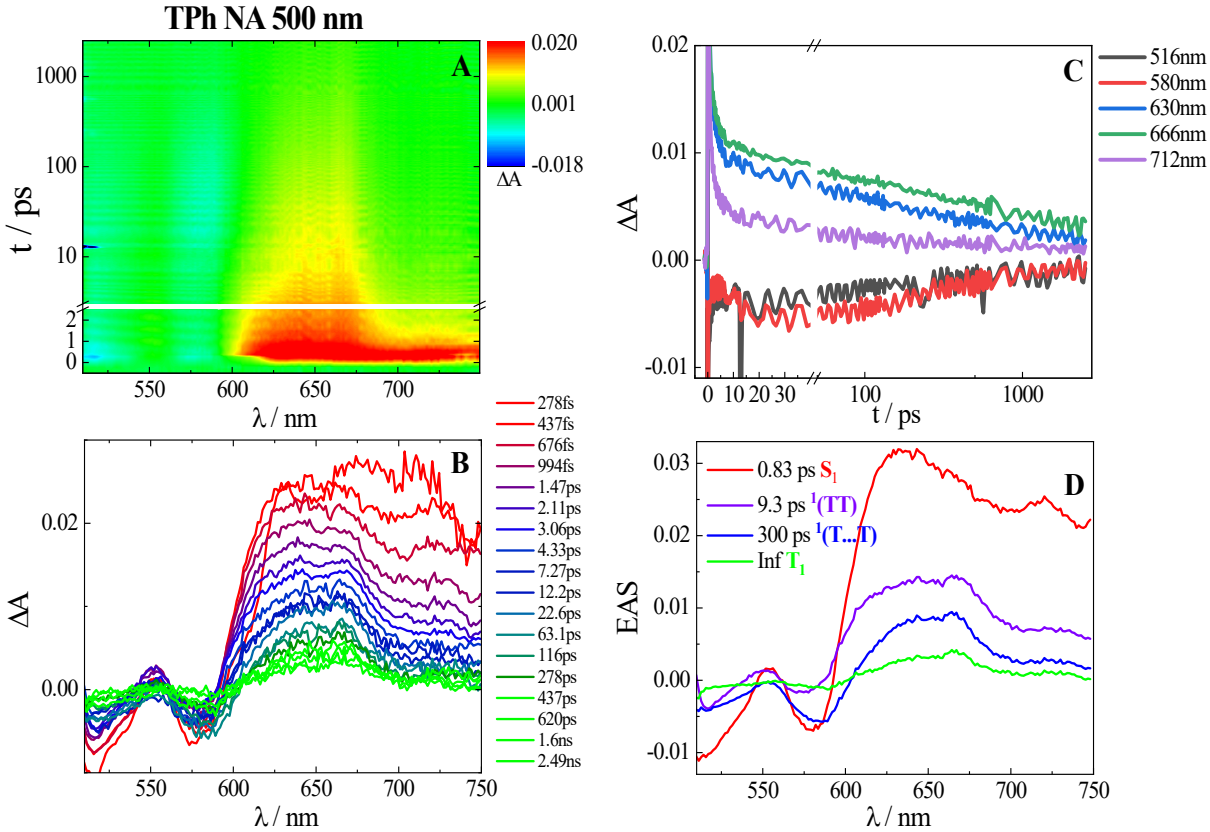

Figure S18. Femtosecond transient absorption matrix (A) spectra at different delay times (B), kinetics at different wavelengths (C), Evolution Associated Spectra (EAS) and lifetimes (D) obtained from Global Fit for **TPh** in water NA upon excitation at 500 nm with a laser fluence of 190 μJ/cm².

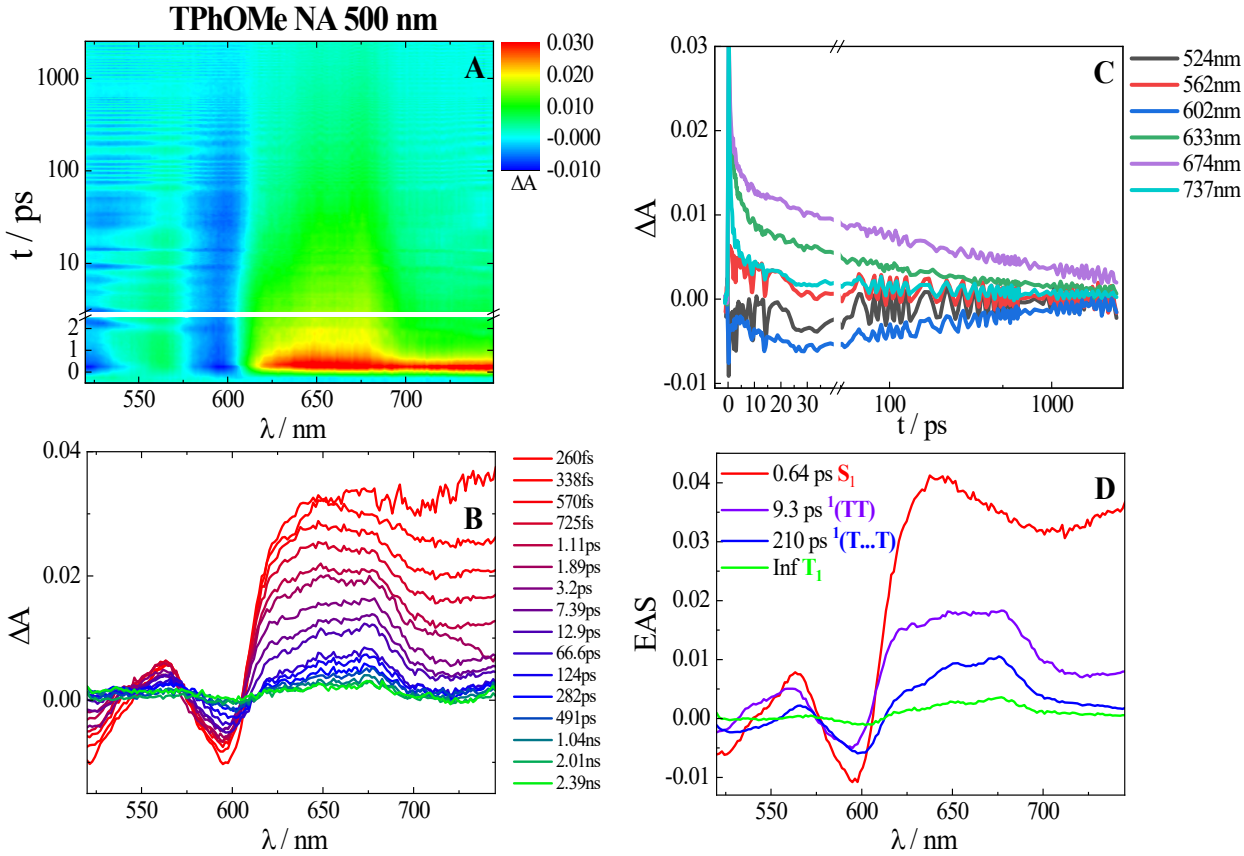

Figure S19. Femtosecond transient absorption matrix (A) spectra at different delay times (B), kinetics at different wavelengths (C), Evolution Associated Spectra (EAS) and lifetimes (D) obtained from Global Fit for **TPhOMe** in water NA upon excitation at 500 nm with a laser fluence of 190 μJ/cm².

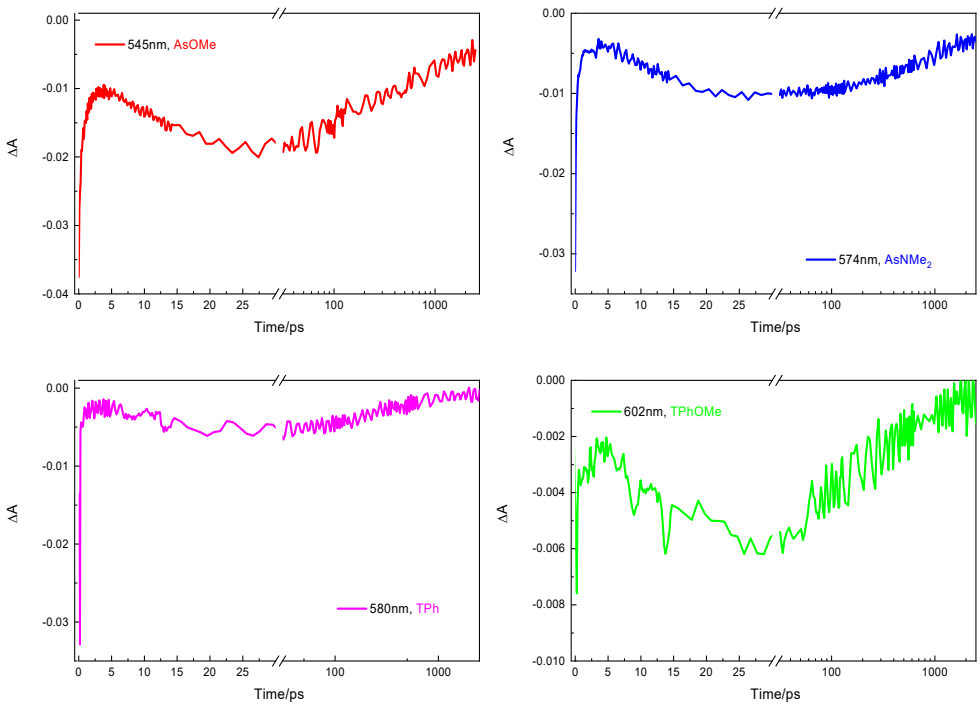

Figure S20. Femtosecond transient absorption results upon excitation at 500 nm with a laser fluence of 190 μJ/cm^2: kinetics obtained for the water-dispersed NA of the investigated compounds in correspondence with the J-aggregate ground state bleaching.

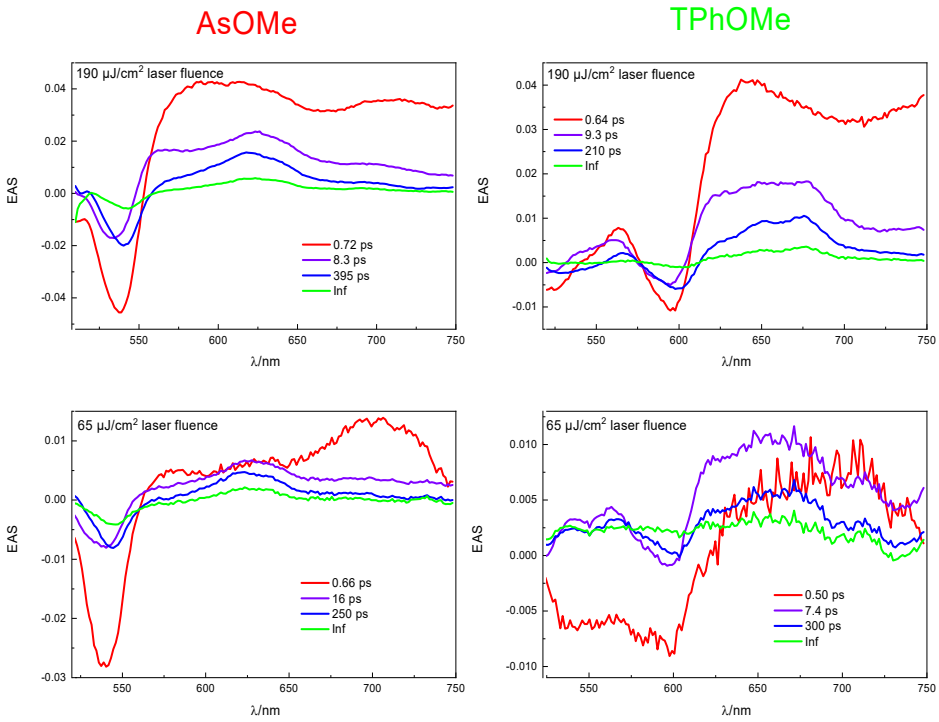

Figure S21. Femtosecond transient absorption results, Evolution Associated Spectra (EAS), and lifetimes obtained from Global Analysis for the water-dispersed NA of **AsOMe** and **TPhOMe** upon excitation at 500 nm at two different laser fluences of 190 and 65 μJ/cm^2.

Triplet Yield Calculation

Triplet yields were evaluated from the temporal dynamics of the lowest excited singlet and triplet state populations, as obtained through analysis of the femtosecond transient absorption data, according to a procedure already described in the literature, and here detailed for the water-dispersed nanoaggregates of the investigated compounds.[12,13]

AsOMe exc 400 nm

Global Fitting of the femtosecond transient absorption data was carried out using the Glotaran software which provided us with the Evolution Associated Spectra of the four exponential components and their temporal composition (Figure S22).

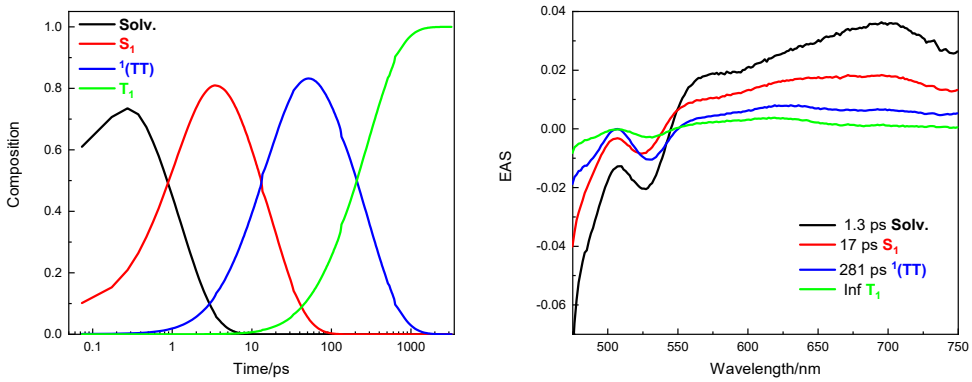

Figure S22. Evolution-Associated Spectra (right) and composition in time (left) of the four exponential components resulting from the global fitting of the femtosecond transient absorption data of **AsOMe** nanoaggregates in water dispersion.

To obtain the spectral shapes of the excited singlet and triplet states, the transient spectra at time delays of 3.5 and 3000 ps were selected, respectively (Figure S23). In fact, at these time delays abundances of the singlet and triplet transients were at their maxima ΔA value in the femtosecond transient absorption data (Figure S22, right side).

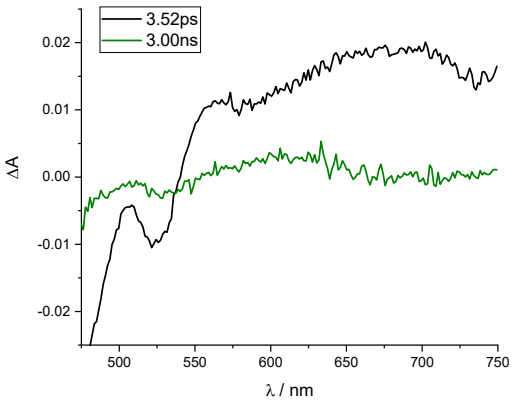

Figure S23. Transient absorption spectra at 3.52 and 3000 ps time delays from excitation recorded for **AsOMe** nanoaggregates in water.

The spectra of the lowest singlet and triplet excited states must be related through the GSB they share in common. The ground state absorption spectrum was scaled and subtracted from the 3.52/3000 ps transient spectra in order to remove the GSB contribution. The ground state absorption spectrum was normalized to the transient absorption spectrum at the peak of the ground state bleaching, and then subtracted. The normalization was the method employed to determine the "right" amount of ground-state absorption to be subtracted each time. The resulting spectra only show the S_1/T_1 ESA relative to a known amount of GSB (Figure S24).

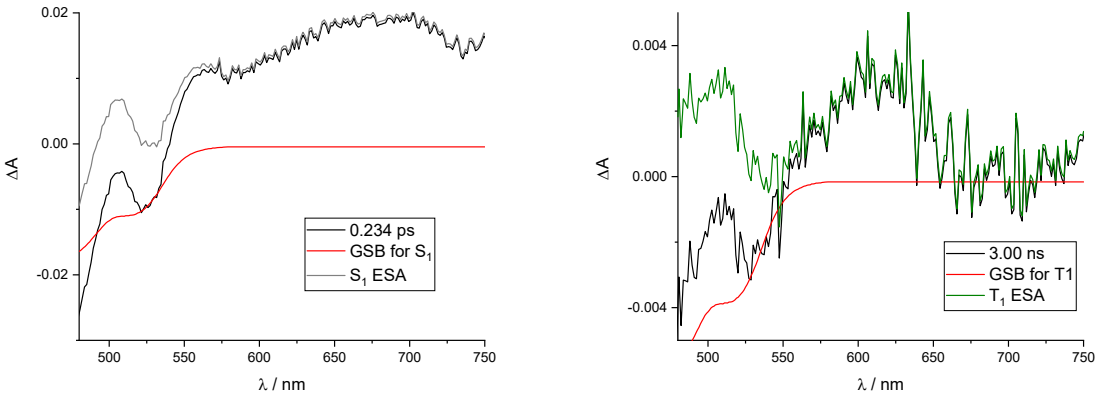

Figure S24. Transient (black) and steady state (red) absorption spectra used to reconstruct the absorption spectra of the excited singlet (grey, left) and triplet (green, right) states.

The S_1 and T_1 spectra are then normalized to the GSB they share, resulting in two spectra that are quantitatively related (Figure S25).

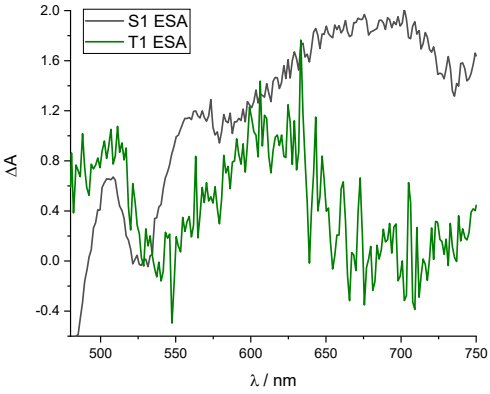

Figure S25. Excited-state absorption spectra, normalized to GSB, used to correct the composition profile in Figure S22 and to obtain population dynamics in Figure S26.

The quantitatively related spectra of S_1 and T_1 were used to correct the composition profiles previously shown. The temporal composition of the components resulting from the global fitting reported in Figure S22 is indeed related to the differential absorbance measured during the ultrafast absorption experiments. Therefore, according to the Lambert−Beer law, it is dependent on both the absorption ability and the concentration of S_1 and T_1. From the quantitatively related S_1 and T_1 spectra reported in Figure S25, it is clear that the ratio between the triplet excited state absorption at its peak (1.10 at 625 nm) and the singlet excited state absorption at its peak (1.90 at 700 nm) is $\frac{\varepsilon_T}{\varepsilon_S} = 0.579$. By scaling the S_1 and T_1 temporal compositions in Figure S22 (left side) for this factor (multiplying the singlet profile by 0.579), the correct concentration profiles were obtained: $\frac{c_S}{c_T} = \frac{\Delta A_S}{\Delta A_T} \times \frac{\varepsilon_T}{\varepsilon_S}$. From the population profiles normalized at the singlet population peak (Figure S26), a triplet quantum yield of **214%** was estimated for **AsOMe** nanoaggregates in water.

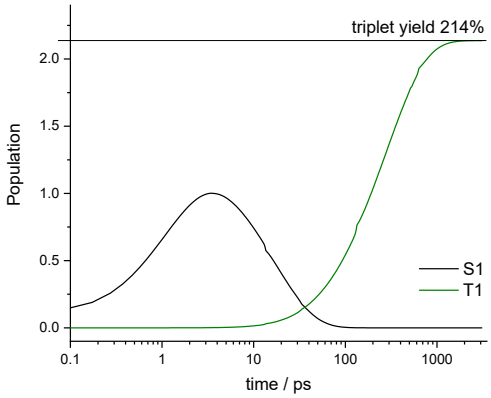

Figure S26. Population dynamics of the excited singlet and triplet states for **AsOMe** nanoaggregates in water upon 400 nm excitation with a laser fluence of 300 μJ/cm^2.

AsNMe$_2$ exc 400 nm

Global Fitting of the femtosecond transient absorption data was carried out using the Glotaran software, which provided us with the Evolution Associated Spectra of the four exponential components and their temporal composition (Figure S27).

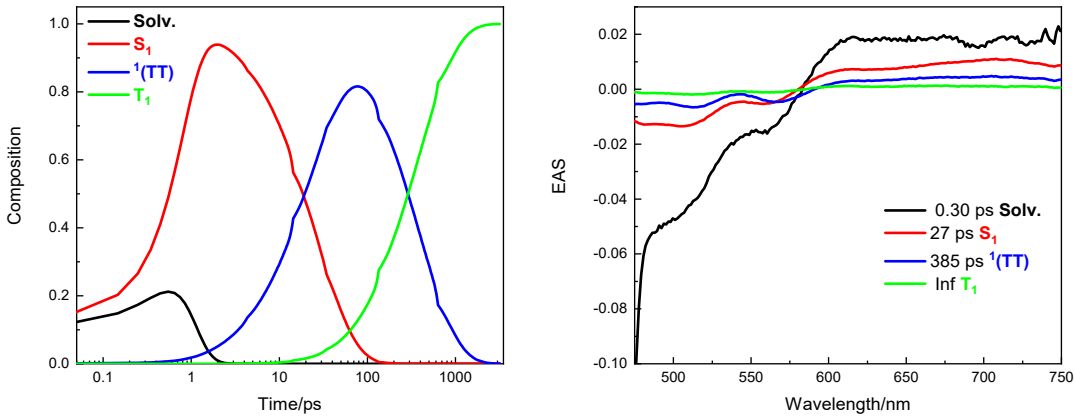

Figure S27. Evolution-Associated Spectra (right) and composition in time (left) of the four exponential components resulting from the global fitting of the femtosecond transient absorption data of **AsNMe$_2$** nanoaggregates in water.

To obtain the spectral shapes of the excited singlet and triplet states, the transient spectra at time delays of 2.05 and 3000 ps were selected, respectively (Figure S28). In fact, at these time delays abundances of the singlet and triplet transients were at the maxima A value in the femtosecond transient absorption data (Figure S27, right side).

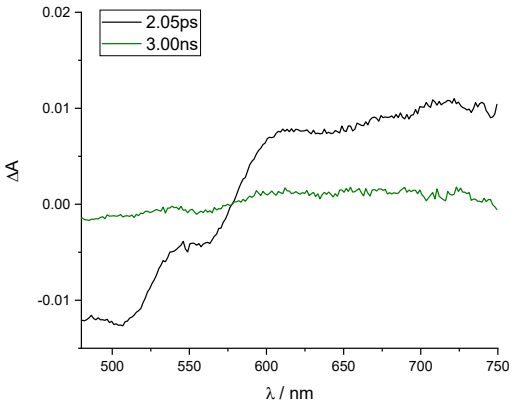

Figure S28. Transient absorption spectra at 2.05 and 3000 ps time delays from excitation recorded for **$AsNMe_2$** nanoaggregates in water.

The spectra of the lowest singlet and triplet excited states must be related through the GSB they share in common. The ground state absorption spectrum was scaled and subtracted from the 2.05/3000 ps transient spectra in order to remove the GSB contribution. The ground state absorption spectrum was normalized to the transient absorption spectrum at the peak of the ground state bleaching, and then subtracted. The normalization was the method employed to determine the "right" amount of ground-state absorption to be subtracted each time. The resulting spectra only show the S_1/T_1 ESA relative to a known amount of GSB (Figure S29).

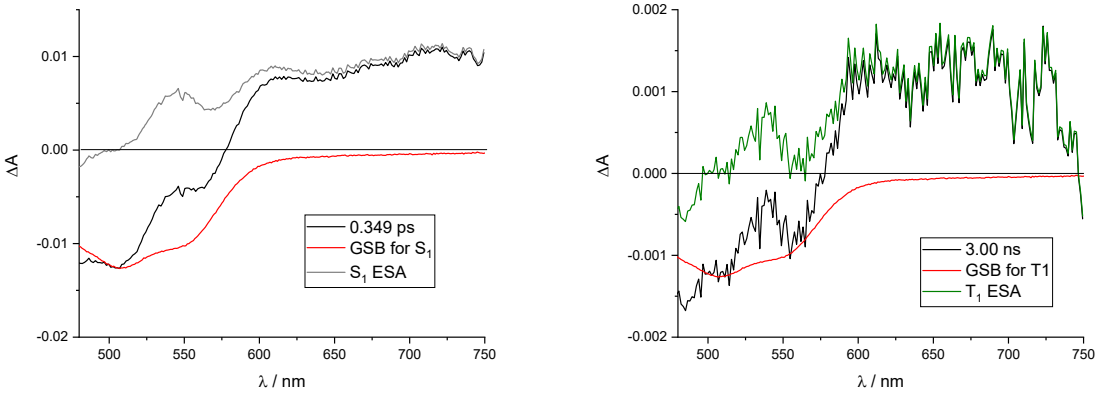

Figure S29. Transient (black) and steady state (red) absorption spectra used to reconstruct the absorption spectra of the excited singlet (grey, left) and triplet (green, right) states.

The S_1 and T_1 spectra are then normalized to the GSB they share, resulting in two spectra that are quantitatively related (Figure S30).

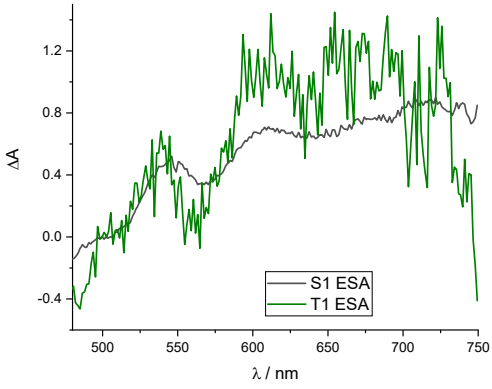

Figure S30. Excited state absorption spectra, normalized to GSB, used to correct the composition profile in Figure S27 and to obtain population dynamics in Figure S31.

The quantitatively related spectra of S_1 and T_1 were used to correct the composition profiles previously shown. The temporal composition of the components resulting from the global fitting reported in Figure S27 is indeed related to the differential absorbance measured during the ultrafast absorption experiments. Therefore, according to the Lambert−Beer law, it is dependent on both the absorption ability and the concentration of S_1 and T_1. From the quantitatively related S_1 and T_1 spectra reported in Figure S30, it is clear that the ratio between the triplet excited state absorption at its peak (ca. 1.03 at 610 nm) and the singlet excited state absorption at its peak (0.883 at 720 nm) is $\frac{\varepsilon_T}{\varepsilon_S} = 1.17$. By scaling the S_1 and T_1 temporal compositions in Figure S27 (left side) for this factor (multiplying the singlet profile by 1.17), the correct concentration profiles were obtained: $\frac{c_S}{c_T} = \frac{\Delta A_S}{\Delta A_T} \times \frac{\varepsilon_T}{\varepsilon_S}$. From the population profiles normalized at the singlet population peak (Figure S31), a triplet quantum yield of ca. **91%** was estimated for **$AsNMe_2$** nanoaggregates in water.

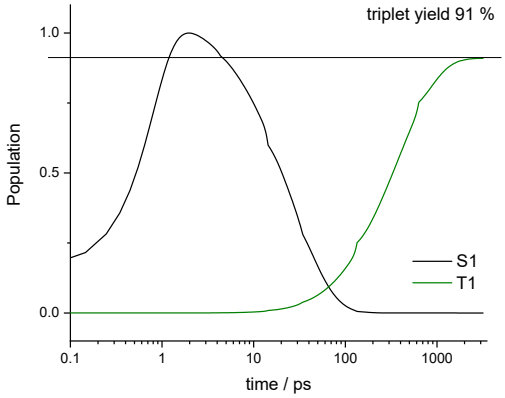

Figure S31. Population dynamics of the excited singlet and triplet states for **$AsNMe_2$** nanoaggregates in water upon 400 nm excitation with a laser fluence of 300 μJ/cm^2.

TPh exc 400 nm

Global Fitting of the femtosecond transient absorption data was carried out using the Glotaran software, which provided us with the Evolution Associated Spectra of the four exponential components and their temporal composition (Figure S32).

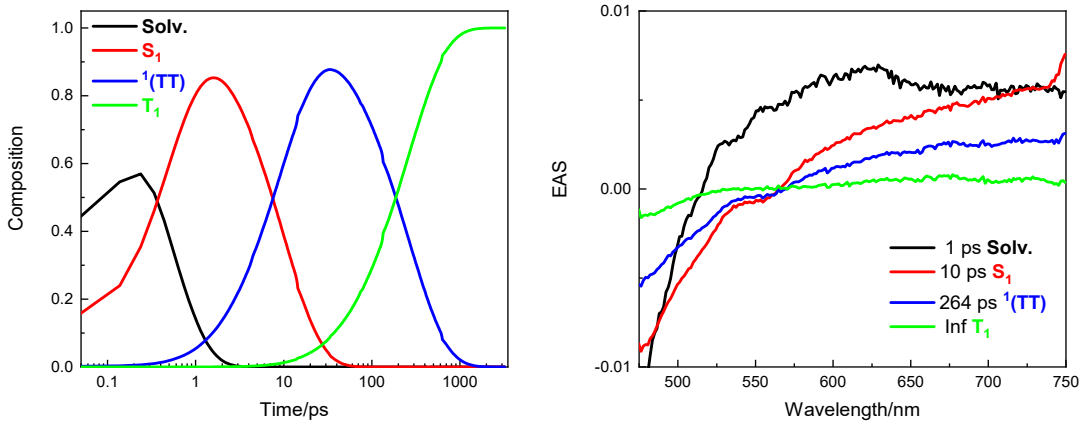

Figure S32. Evolution-Associated Spectra (right) and composition in time (left) of the four exponential components resulting from the global fitting of the femtosecond transient absorption data of **TPh** nanoaggregates in water.

To obtain the spectral shapes of the excited singlet and triplet states the transient spectra at time delays of 1.57 and 2460 ps were selected, respectively (Figure S33). In fact, at these time delays, abundances of the singlet and triplet transients were at the maxima ΔA value in the femtosecond transient absorption data (Figure S32, right side).

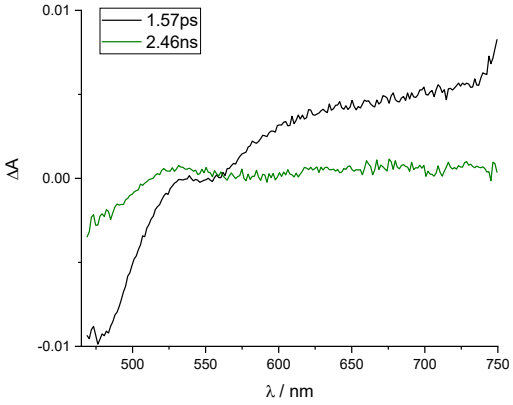

Figure S33. Transient absorption spectra at 1.57 and 2460 ps time delays from excitation recorded for **TPh** nanoaggregates in water.

The spectra of the lowest singlet and triplet excited states must be related through the GSB they share in common. The ground state absorption spectrum was scaled and subtracted from the 1.57/2460 ps transient spectra in order to remove the GSB contribution. The ground state absorption spectrum was normalized to the transient absorption spectrum at the peak of the ground state bleaching, and then subtracted. The normalization was the method employed to determine the "right" amount of ground state absorption to be subtracted each time. The resulting spectra only show the S_1/T_1 ESA relative to a known amount of GSB (Figure S34).

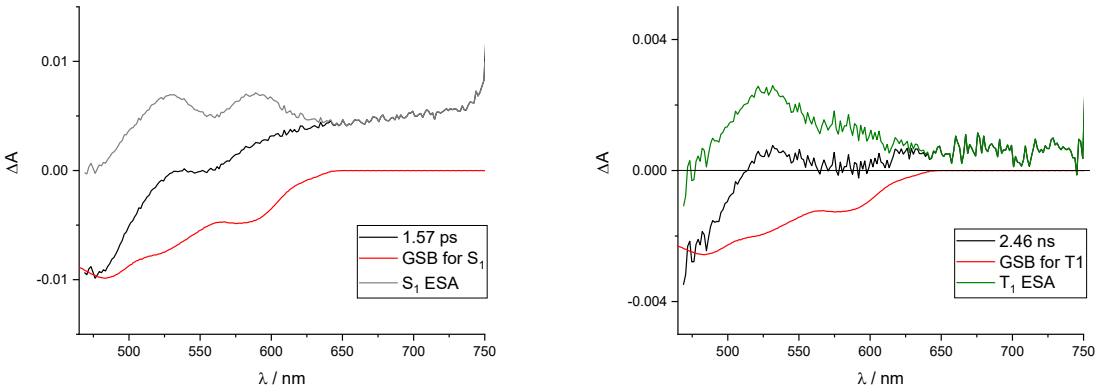

Figure S34. Transient (black) and steady state (red) absorption spectra used to reconstruct the absorption spectra of the excited singlet (grey, left) and triplet (green, right) states.

The S_1 and T_1 spectra are then normalized to the GSB they share, resulting in two spectra that are quantitatively related (Figure S35).

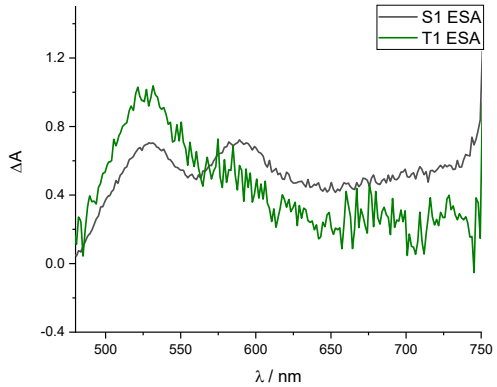

Figure S35. Excited state absorption spectra, normalized to GSB, used to correct the composition profile in Figure S32 and to obtain population dynamics in Figure S36.

The quantitatively related spectra of S_1 and T_1 were used to correct the composition profiles previously shown. The temporal composition of the components resulting from the global fitting reported in Figure S32 is indeed related to the differential absorbance measured during the ultrafast absorption experiments. Therefore, according to the Lambert−Beer law, it is dependent on both the absorption ability and the concentration of S_1 and T_1. From the quantitatively related S_1 and T_1 spectra reported in Figure S35, it is clear that the ratio between the triplet excited state absorption at its peak (0.331 at 680 nm) and the singlet excited state absorption at its peak (0.571 at 730 nm) is $\frac{\varepsilon_T}{\varepsilon_S} = 0.580$. By scaling the S_1 and T_1 temporal compositions in Figure S32 (left side) for this factor (multiplying the singlet profile by 0.579), the correct concentration profiles were obtained: $\frac{c_S}{c_T} = \frac{\Delta A_S}{\Delta A_T} \times \frac{\varepsilon_T}{\varepsilon_S}$. From the population profiles normalized at the singlet population peak (Figure S36), a triplet quantum yield of **<u>201%</u>** was estimated for **TPh** nanoaggregates in water.

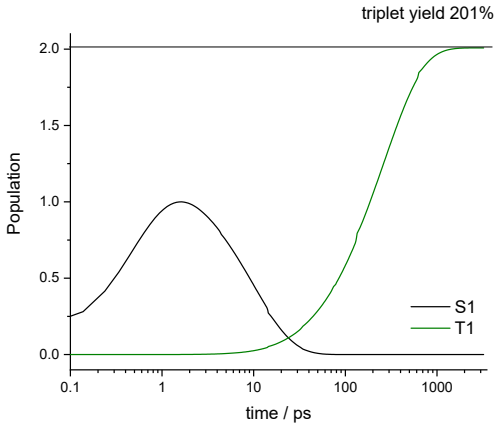

Figure S36. Population dynamics of the excited singlet and triplet states for **TPh** nanoaggregates in water upon 400 nm excitation with a laser fluence of 300 μJ/cm^2.

<u>TPhOMe exc 400 nm</u>

Global Fitting of the femtosecond transient absorption data was carried out using the Glotaransoftware which provided us with the Evolution Associated Spectra of the four exponential components and their temporal composition (Figure S37).

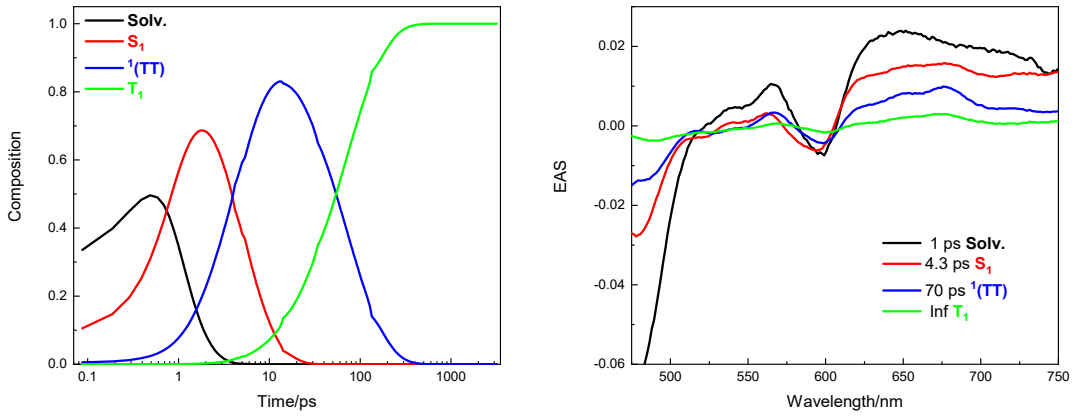

Figure S37. Evolution-Associated Spectra (right) and composition in time (left) of the four exponential components resulting from the global fitting of the femtosecond transient absorption data of **TPhOMe** nanoaggregates in water.

To obtain the spectral shapes of the excited singlet and triplet states, the transient spectra at time delays of 1.78 and 1750 ps were selected, respectively (Figure S38). In fact, at these time delays abundances of the singlet and triplet transients were at the maxima ΔA value in the femtosecond transient absorption data (Figure S37, right side).

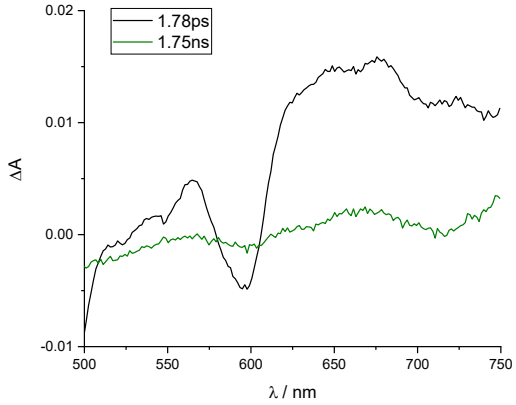

Figure S38. Transient absorption spectra at 1.78 and 1750 ps time delays from excitation recorded for **TPhOMe** nanoaggregates in water.

The spectra of the lowest singlet and triplet excited states must be related through the GSB they share in common. The ground state absorption spectrum was scaled and subtracted from the 1.78/1750 ps transient spectra in order to remove the GSB contribution. The ground state absorption spectrum was normalized to the transient absorption spectrum at the peak of the ground state bleaching, and then subtracted. The normalization was the method employed to determine the "right" amount of ground-state absorption to be subtracted each time. The resulting spectra only show the S_1/T_1 ESA relative to a known amount of GSB (Figure S39).

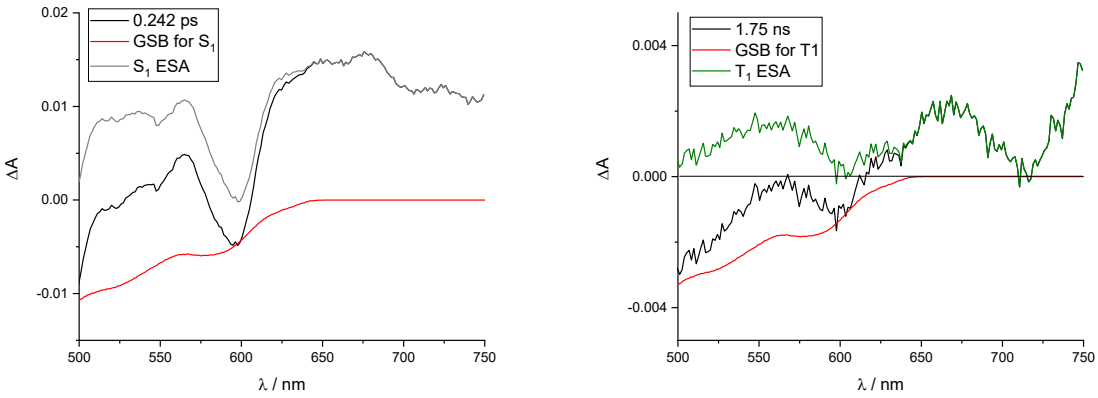

Figure S39. Transient (black) and steady state (red) absorption spectra used to reconstruct the absorption spectra of the excited singlet (grey, left) and triplet (green, right) states.

The S_1 and T_1 spectra are then normalized to the GSB they share, resulting in two spectra that are quantitatively related (Figure S40).

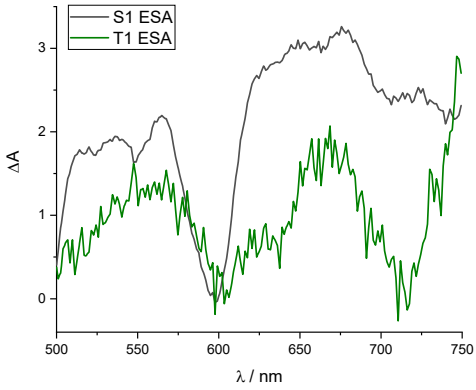

Figure S40. Excited state absorption spectra, normalized to GSB, used to correct the composition profile in Figure S37 and to obtain population dynamics in Figure S41.

The quantitatively related spectra of S_1 and T_1 were used to correct the composition profiles previously shown. The temporal composition of the components resulting from the global fitting reported in Figure S37 is indeed related to the differential absorbance measured during the ultrafast absorption experiments. Therefore, according to the Lambert−Beer law, it is dependent on both the absorption ability and the concentration of S_1 and T_1. From the quantitatively related S_1 and T_1 spectra reported in Figure S40, it is clear that the ratio between the triplet excited state absorption at its peak (1.80at 670 nm) and the singlet excited state absorption at its peak (2.50 at 725 nm) is $\frac{\varepsilon_T}{\varepsilon_S} = 0.72$. By scaling the S_1 and T_1 temporal compositions in Figure S37 (left side) for this factor (multiplying the singlet profile by 0.72), the correct concentration profiles were obtained: $\frac{c_S}{c_T} = \frac{\Delta A_S}{\Delta A_T} \times \frac{\varepsilon_T}{\varepsilon_S}$. From the population profiles normalized at the singlet population peak (Figure S41), a triplet quantum yield of **202%** was estimated for **TPhOMe** nanoaggregates in water.

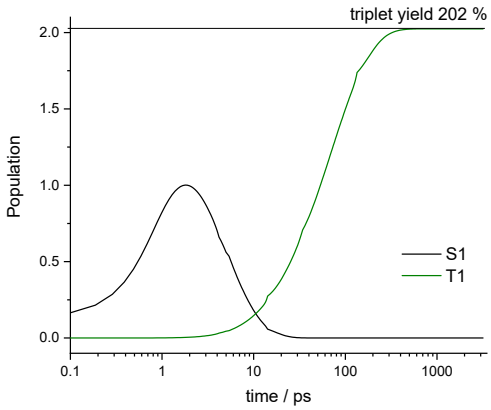

Figure S41. Population dynamics of the excited singlet and triplet states for **TPhOMe** nanoaggregates in water upon 400 nm excitation with a laser fluence of 300 μJ/cm^2.

AsOMe exc 500 nm laser fluence of 190 μJ/cm^2

Global Fitting of the femtosecond transient absorption data was carried out using the Glotaran software which provided us with the Evolution Associated Spectra of the four exponential components and their temporal composition (Figure S42).

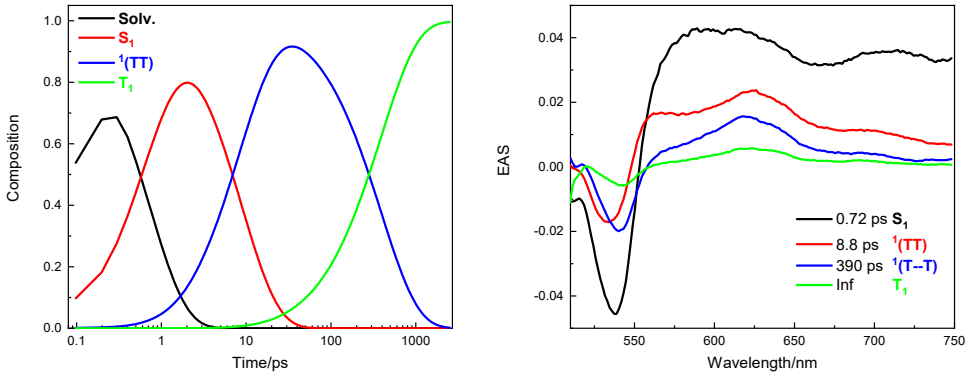

Figure S42. Evolution Associated Spectra (right) and composition in time (left) of the four exponential components resulting from global fitting of the femtosecond transient absorption data of **AsOMe** nanoaggregates in water dispersion upon 500 nm excitation with a laser fluence of 190 μJ/cm^2.

To obtain the spectral shapes of the excited singlet and triplet states the transient spectra at time delays of 0.30 and 2400 ps were selected, respectively (Figure S43). In fact, at these time delays abundances of the singlet and triplet transients were at the maxima ΔA value in the femtosecond transient absorption data (Figure S42, right side).

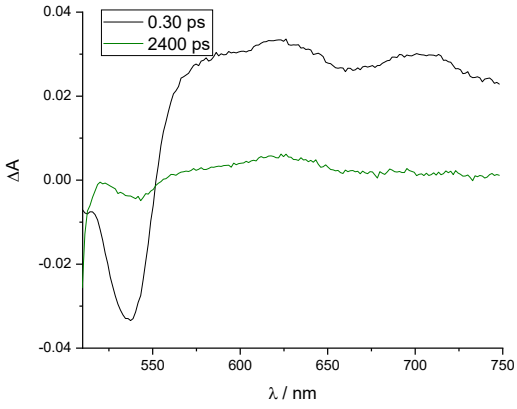

Figure S43. Transient absorption spectra at 0.30 and 2400 ps time delays from excitation recorded for **AsOMe** nanoaggregates in water upon 500 nm excitation with a laser fluence of 190 μJ/cm^2.

The spectra of the lowest singlet and triplet excited states must be related through the GSB they share in common. The ground state absorption spectrum was scaled and subtracted from the 0.30/2400 ps transient spectra in order to remove the GSB

contribution. The ground state absorption spectrum was normalized to the transient absorption spectrum at the peak of the ground-state bleaching, and then subtracted. The normalization was the method employed to determine the "right" amount of ground-state absorption to be subtracted each time. The resulting spectra only show the S_1/T_1 ESA relative to a known amount of GSB (Figure S44).

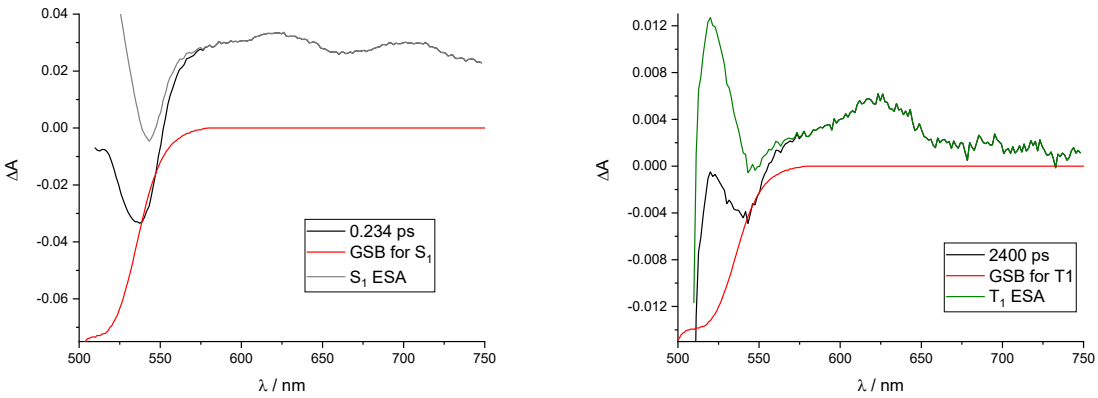

Figure S44. Transient (black) and steady state (red) absorption spectra used to reconstruct the absorption spectra of the excited singlet (grey, left) and triplet (green, right) states.

The S_1 and T_1 spectra are then normalized to the GSB they share, resulting in two spectra that are quantitatively related (Figure S45).

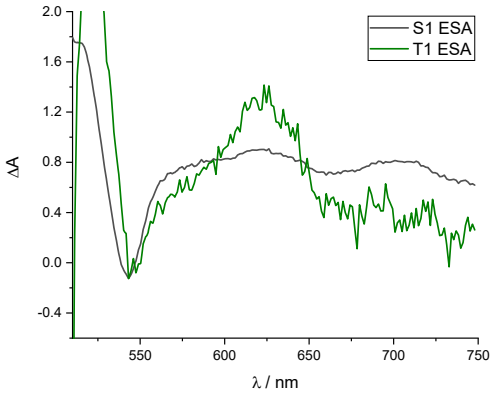

Figure S45. Excited state absorption spectra, normalized to GSB, used to correct the composition profile in Figure S42 and to obtain population dynamics in Figure S46.

The quantitatively related spectra of S_1 and T_1 were used to correct the composition profiles previously shown. The temporal composition of the components resulting from the global fitting reported in Figure S42 is indeed related to the differential absorbance measured during the ultrafast absorption experiments. Therefore, according to the Lambert–Beer law, it is dependent on both the absorption ability and the concentration of S_1 and T_1. From the quantitatively related S_1 and T_1 spectra reported in Figure S45, it is clear that the ratio between the triplet excited state absorption at its peak (1.30 at 620 nm) and the singlet excited state absorption at its peak (0.81 at 700 nm) is $\frac{\varepsilon_T}{\varepsilon_S} = 1.605$. By scaling the S_1 and T_1 temporal compositions in Figure S42 (left side) for this factor (multiplying the singlet profile by 1.605), the correct concentration profiles were obtained: $\frac{c_S}{c_T} = \frac{\Delta A_S}{\Delta A_T} \times \frac{\varepsilon_T}{\varepsilon_S}$. From the population profiles normalized at the singlet population peak (Figure S46), a triplet quantum yield of **<u>90%</u>** was estimated for **AsOMe** nanoaggregates in water upon 500 nm excitation with a laser fluence of 190 μJ/cm^2.

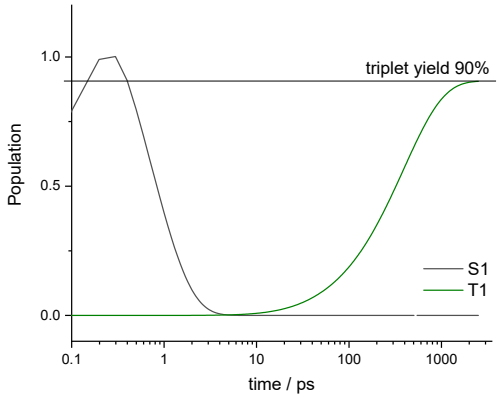

Figure S46. Population dynamics of the excited singlet and triplet states for **AsOMe** nanoaggregates in water upon 500 nm excitation with a laser fluence of 190 μJ/cm^2.

<u>AsOMe exc 500 nm laser fluence of 65 μJ/cm^2</u>

Global Fitting of the femtosecond transient absorption data was carried out using the Glotaran software which provided us with the Evolution Associated Spectra of the four exponential components and their temporal composition (Figure S47).

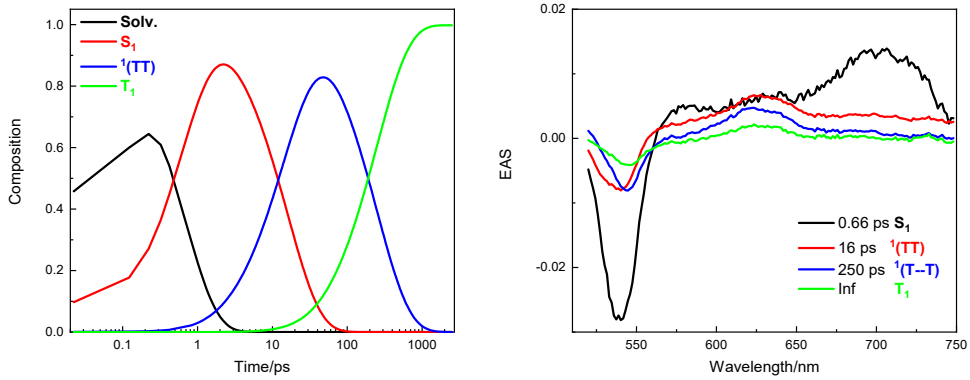

Figure S47. Evolution Associated Spectra (right) and composition in time (left) of the four exponential components resulting from global fitting of the femtosecond transient absorption data of **AsOMe** nanoaggregates in water dispersion upon 500 nm excitation with a laser fluence of 65 μJ/cm^2.

To obtain the spectral shapes of the excited singlet and triplet states the transient spectra at time delays of 0.20 and 2500 ps were selected, respectively (Figure S48). In fact, at these time delays abundances of the singlet and triplet transients were at the maxima ΔA value in the femtosecond transient absorption data (Figure S47, right side).

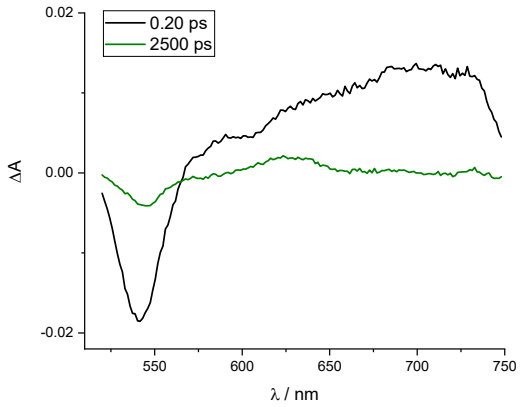

Figure S48. Transient absorption spectra at 0.20 and 2500 ps time delays from excitation recorded for **AsOMe** nanoaggregates in water upon 500 nm excitation with a laser fluence of 65 μJ/cm^2.

The spectra of the lowest singlet and triplet excited states must be related through the GSB they share in common. The ground state absorption spectrum was scaled and subtracted from the 0.20/2500 ps transient spectra in order to remove the GSB contribution. The ground state absorption spectrum was normalized to the transient absorption spectrum at the peak of the

ground-state bleaching, and then subtracted. The normalization was the method employed to determine the "right" amount of ground-state absorption to be subtracted each time. The resulting spectra only show the S_1/T_1 ESA relative to a known amount of GSB (Figure S49).

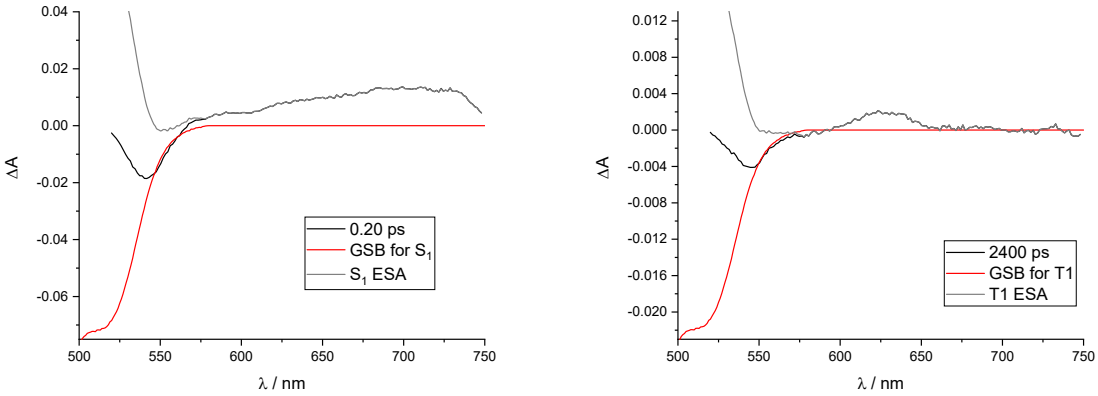

Figure S49. Transient (black) and steady state (red) absorption spectra used to reconstruct the absorption spectra of the excited singlet (grey, left) and triplet (green, right) states.

The S_1 and T_1 spectra are then normalized to the GSB they share, resulting in two spectra that are quantitatively related (Figure S50).

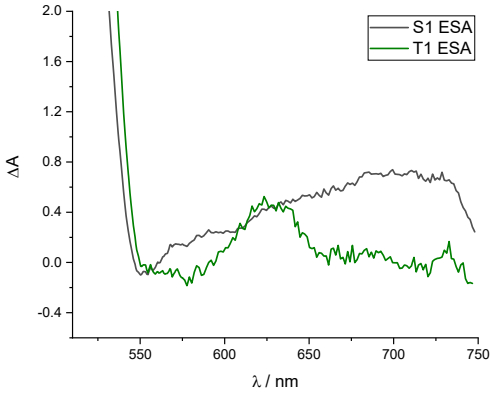

Figure S50. Excited state absorption spectra, normalized to GSB, used to correct the composition profile in Figure S47 and to obtain population dynamics in Figure S51.

The quantitatively related spectra of S_1 and T_1 were used to correct the composition profiles previously shown. The temporal composition of the components resulting from the global fitting reported in Figure S47 is indeed related to the differential absorbance measured during the ultrafast absorption experiments. Therefore, according to the Lambert–Beer law, it is dependent on both the absorption ability and the concentration of S_1 and T_1. From the quantitatively related S_1 and T_1 spectra reported in Figure S50, it is clear that the ratio between the triplet excited state absorption at its peak (0.510 at 625 nm) and the singlet excited state absorption at its peak (0.728 at 710 nm) is $\frac{\varepsilon_T}{\varepsilon_S} = 0.700$. By scaling the S_1 and T_1 temporal compositions in Figure S47 (left side) for this factor (multiplying the singlet profile by 0.700), the correct concentration profiles were obtained: $\frac{c_S}{c_T} = \frac{\Delta A_S}{\Delta A_T} \times \frac{\varepsilon_T}{\varepsilon_S}$. From the population profiles normalized at the singlet population peak (Figure S51), a triplet quantum yield of **<u>220%</u>** was estimated for **AsOMe** nanoaggregates in water upon 500 nm excitation with a laser fluence of 65 μJ/cm^2.

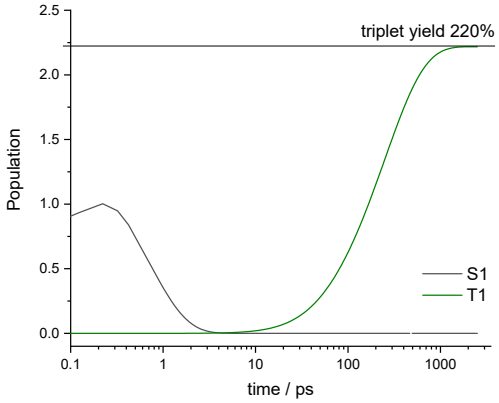

Figure S51. Population dynamics of the excited singlet and triplet states for **AsOMe** nanoaggregates in water upon 500 nm excitation with a laser fluence of 65 μJ/cm^2.

Dynamic Light Scattering

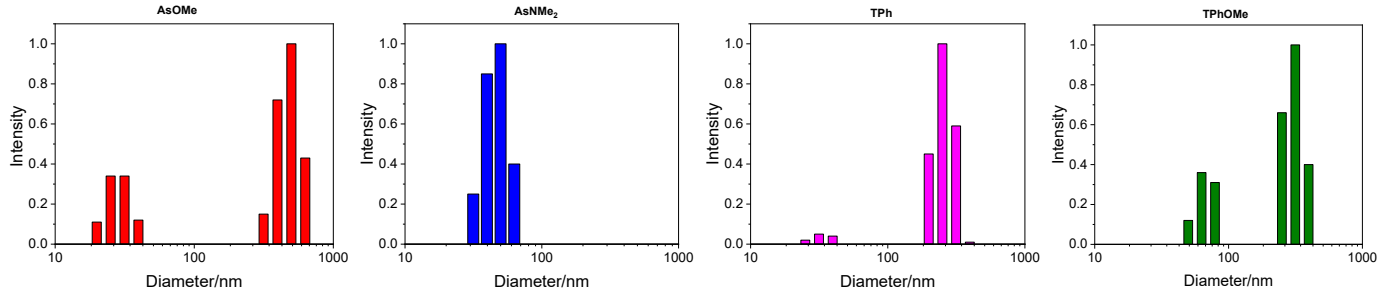

Figure S52. Dynamic Light Scattering (DLS) results showing the size distribution of the nanoaggregates for all the compounds prepared by injection into water of a concentrated DMSO solution.

Table S5. Mean hydrodynamic diameters and relative weight percentages of the nanoaggregates produced upon injection into water of a concentrated DMSO solution obtained from Dynamic Light Scattering (DLS) measurements.

Sample	**Mean diameter / nm**	**Relative weight / %**
AsOMe	28.7	25.4
	479.7	74.6
$AsNMe_2$	46.7	100
TPh	33.4	4.5
	258.6	95.5
TPhOMe	67.2	26.7
	310.2	73.3

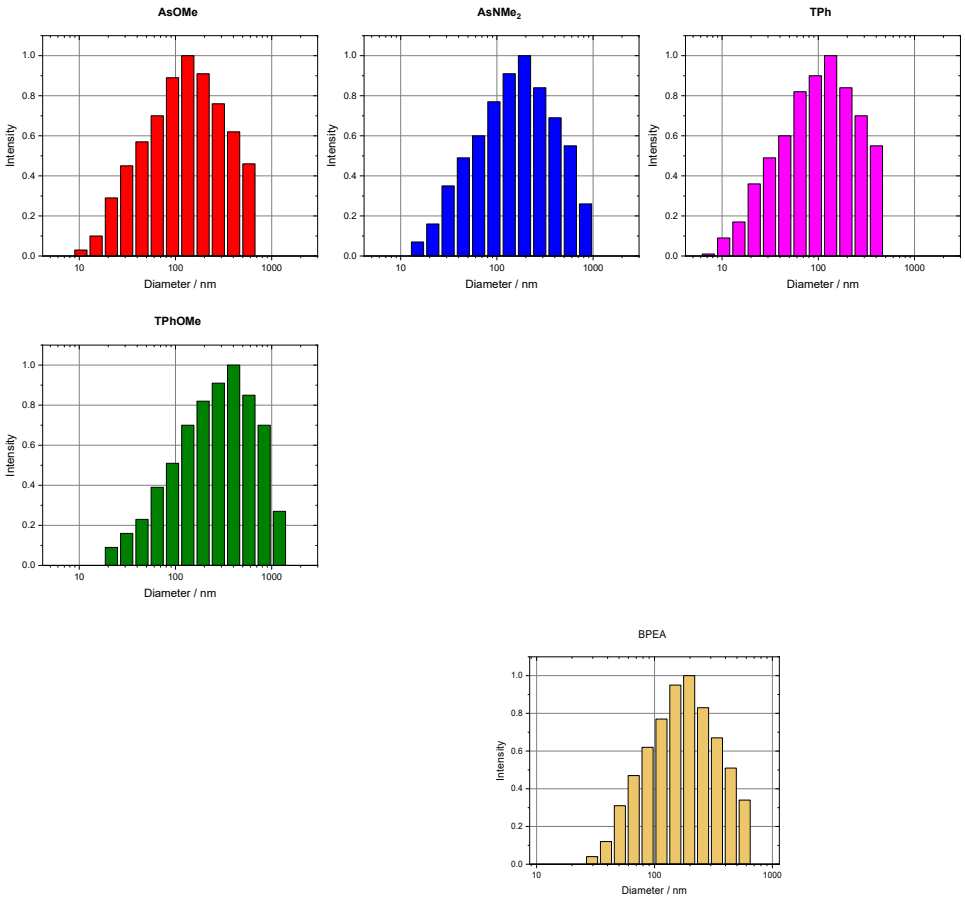

Figure S53. Dynamic Light Scattering (DLS) results showing the size distribution of the nanoaggregates for all the compounds, as well as for the BPEA nanoaggregates used as reference for the ROS fluorimetric tests (see below), prepared by injection into water of a concentrated THF solution upon probe sonication.

Scanning Electron Microscopy

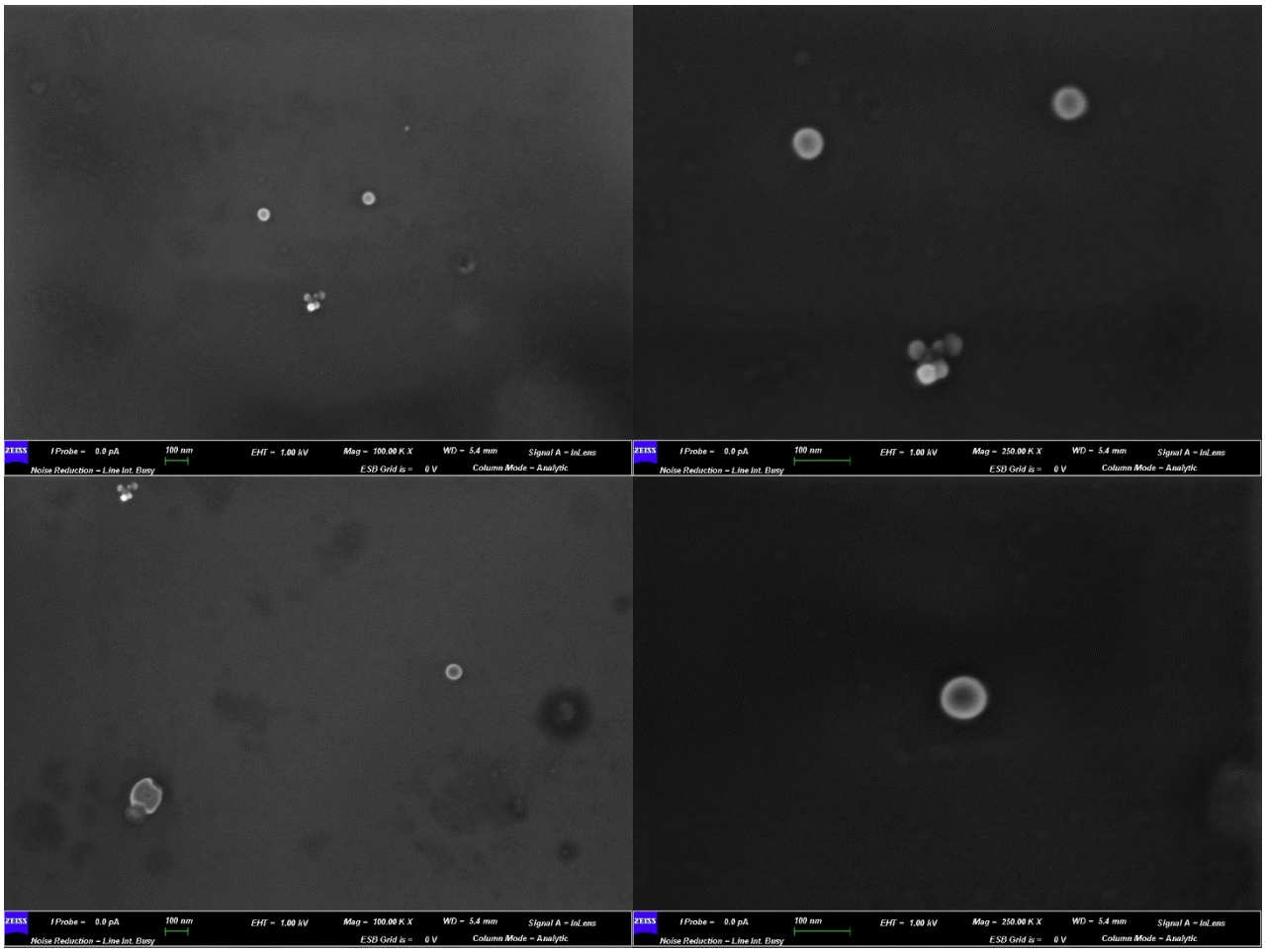

Figure S54.Scanning Electron Microscopy (SEM) images obtained for the **AsOMe** nanoaggregates prepared by injection into water of a 10^{-5} M concentrated THF solution.

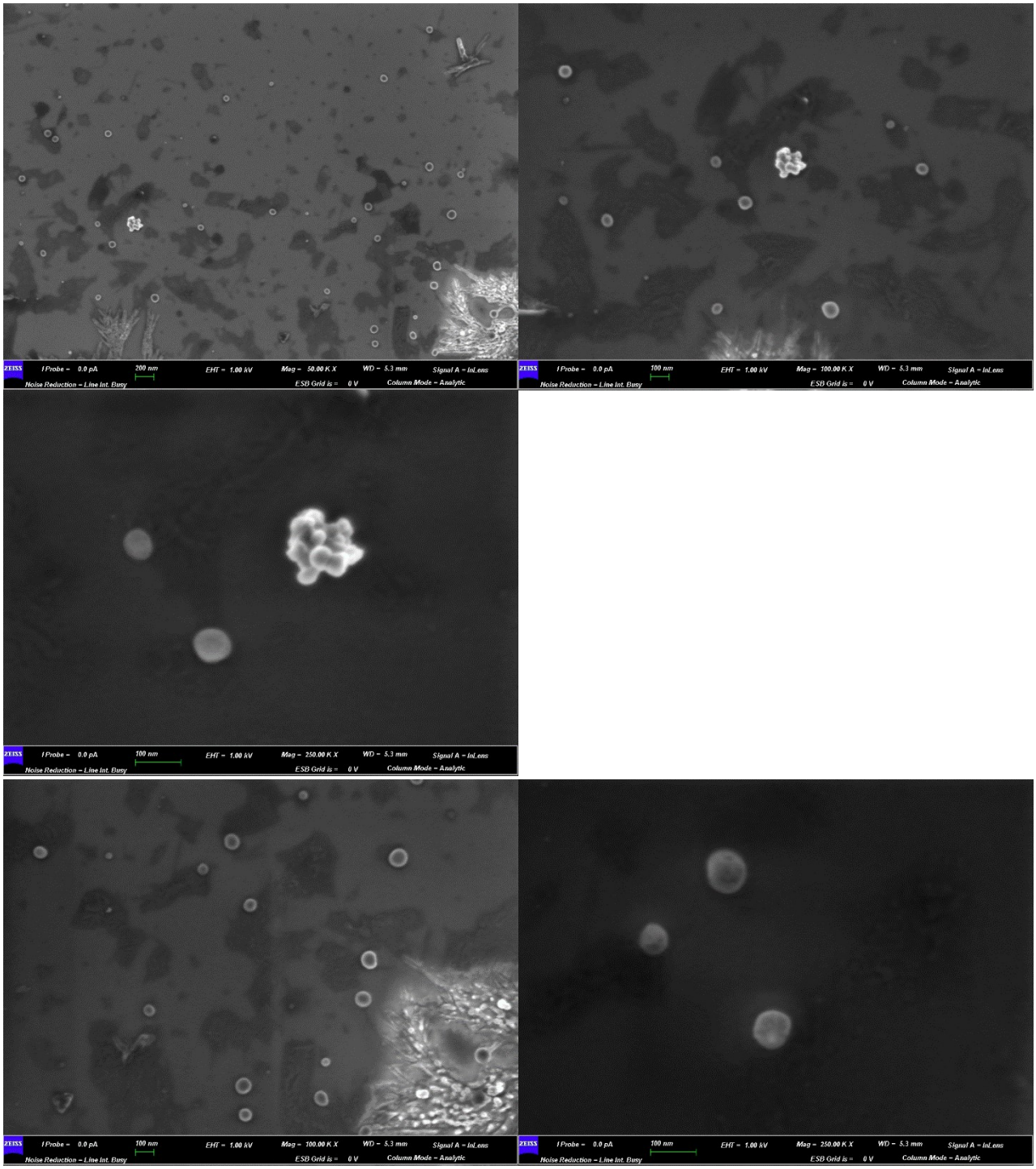

Figure S55.Scanning Electron Microscopy (SEM) images obtained for the **$AsNMe_2$** nanoaggregates prepared by injection into water of a 10^{-5} M concentrated THF solution.

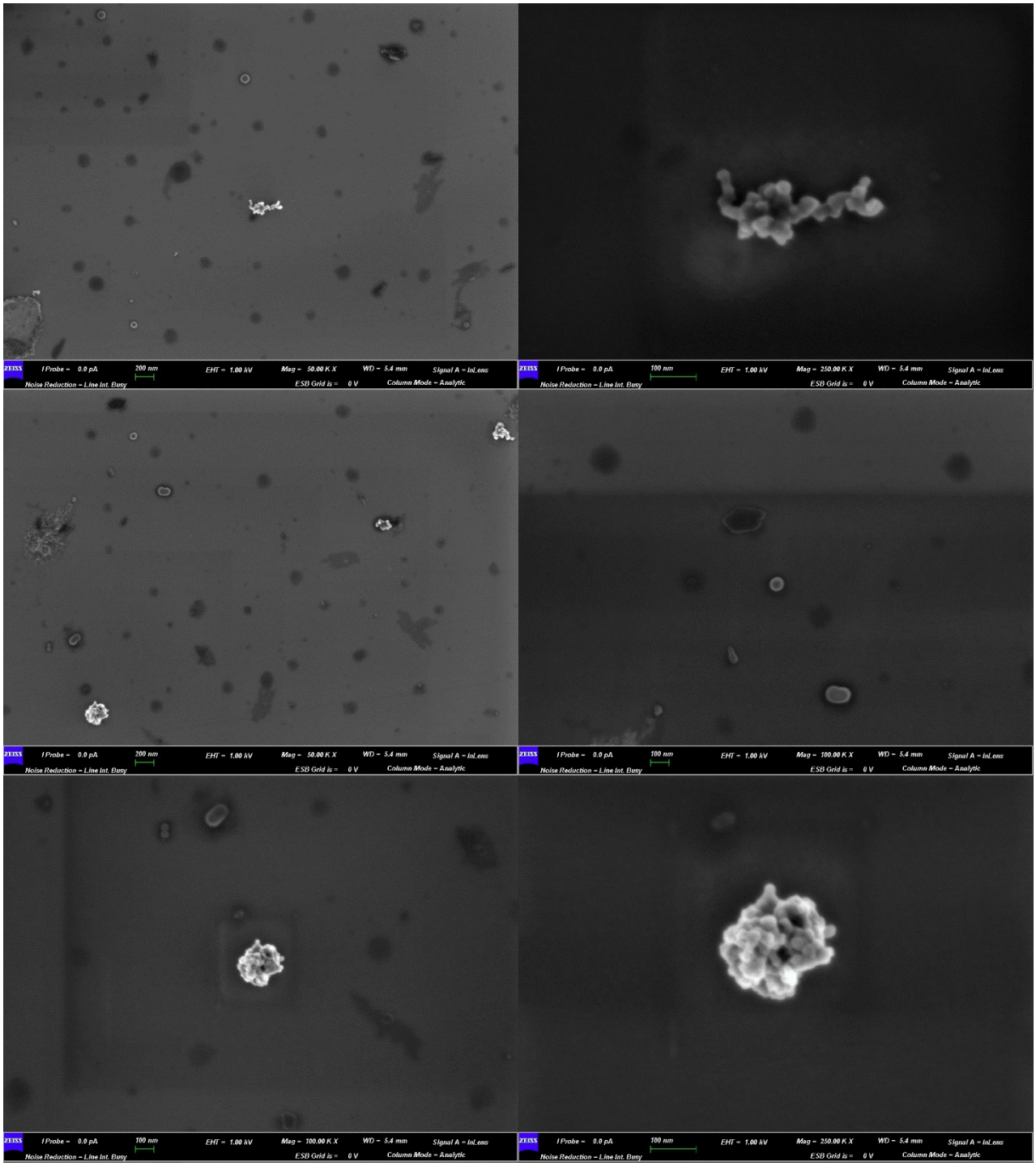

Figure S56. Scanning Electron Microscopy (SEM) images obtained for the **TPh** nanoaggregates prepared by injection into water of a 10^{-6} M concentrated THF solution.

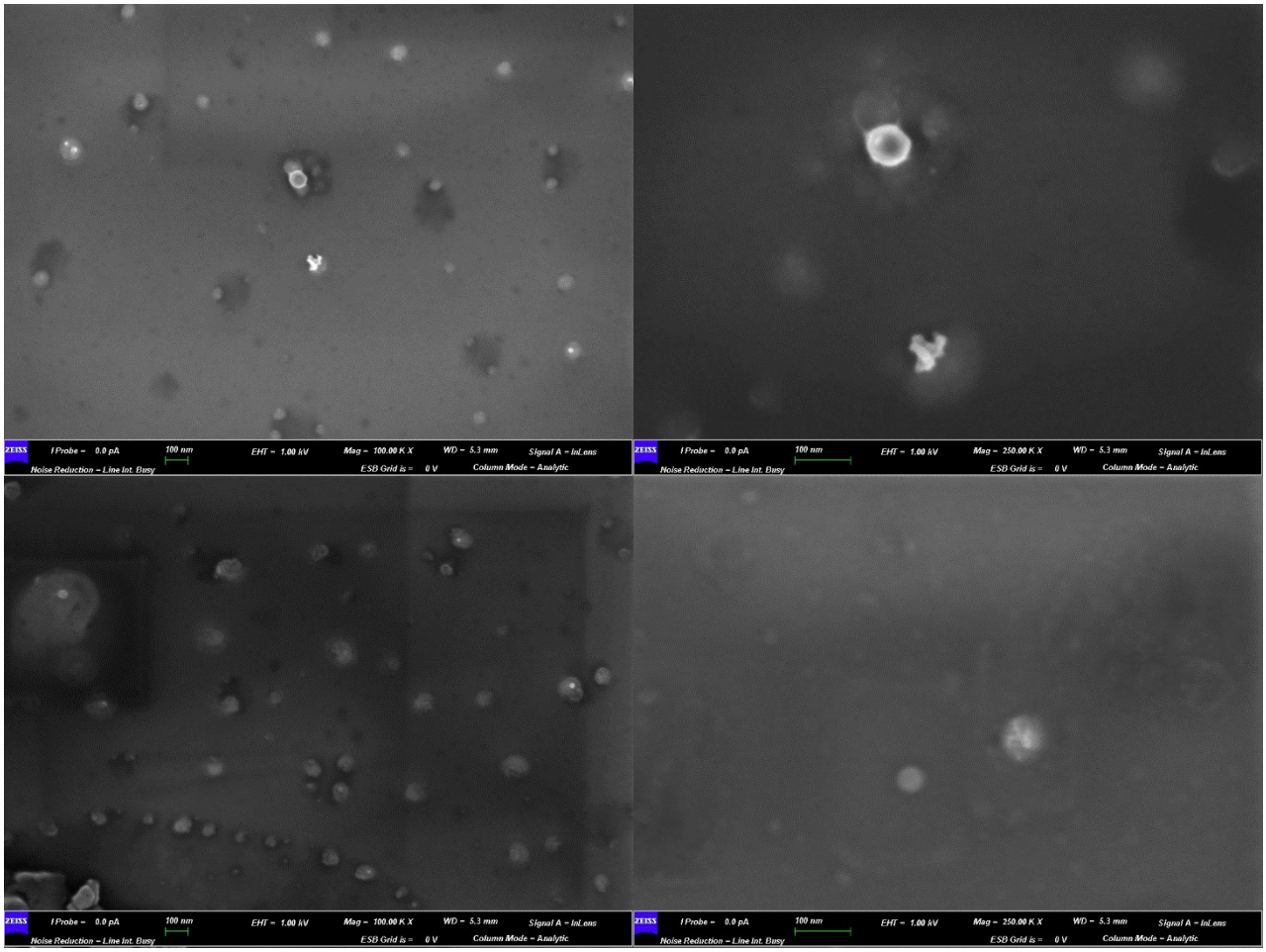

Figure S57. Scanning Electron Microscopy (SEM) images obtained for the **TPhOMe** nanoaggregates prepared by injection into water of a 10^{-6} M concentrated THF solution.

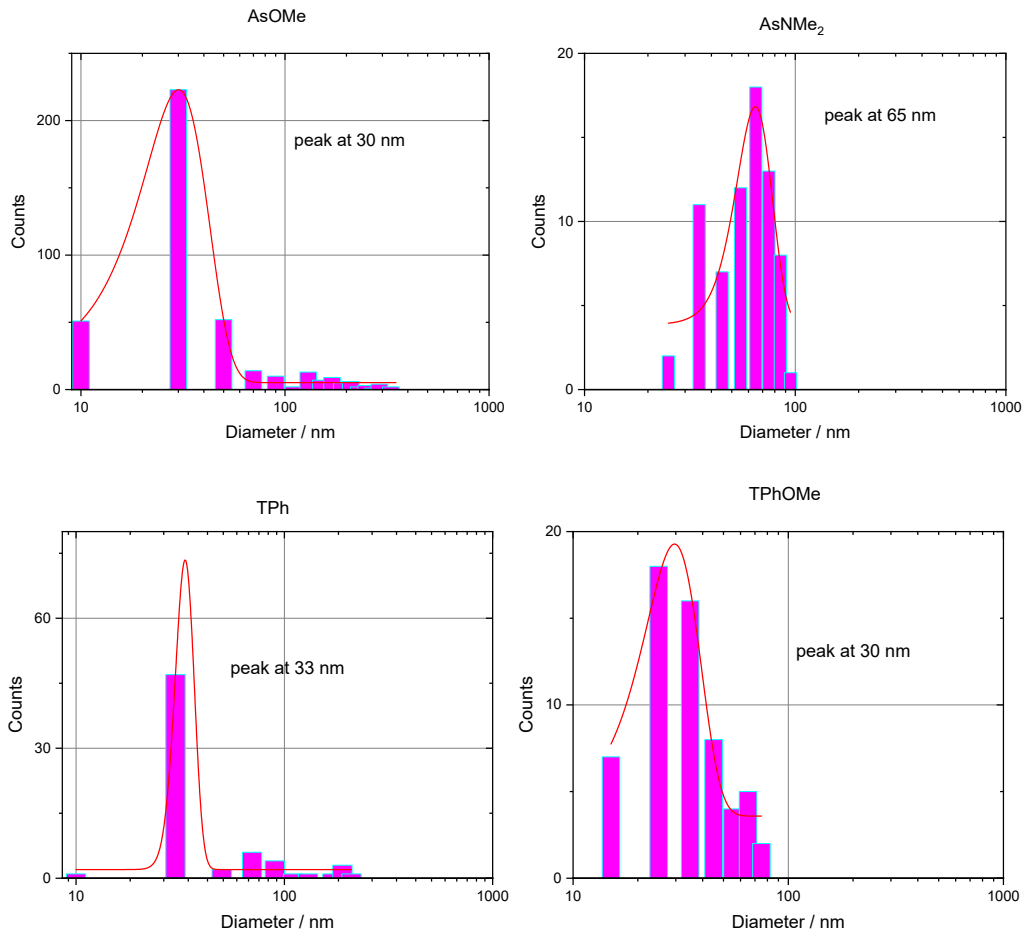

Figure S58. Size distribution of the nanoaggregates for all the compounds prepared by injection into water of a concentrated THF solution obtained from the Scanning Electron Microscopy (SEM) images.

Biological Experiments

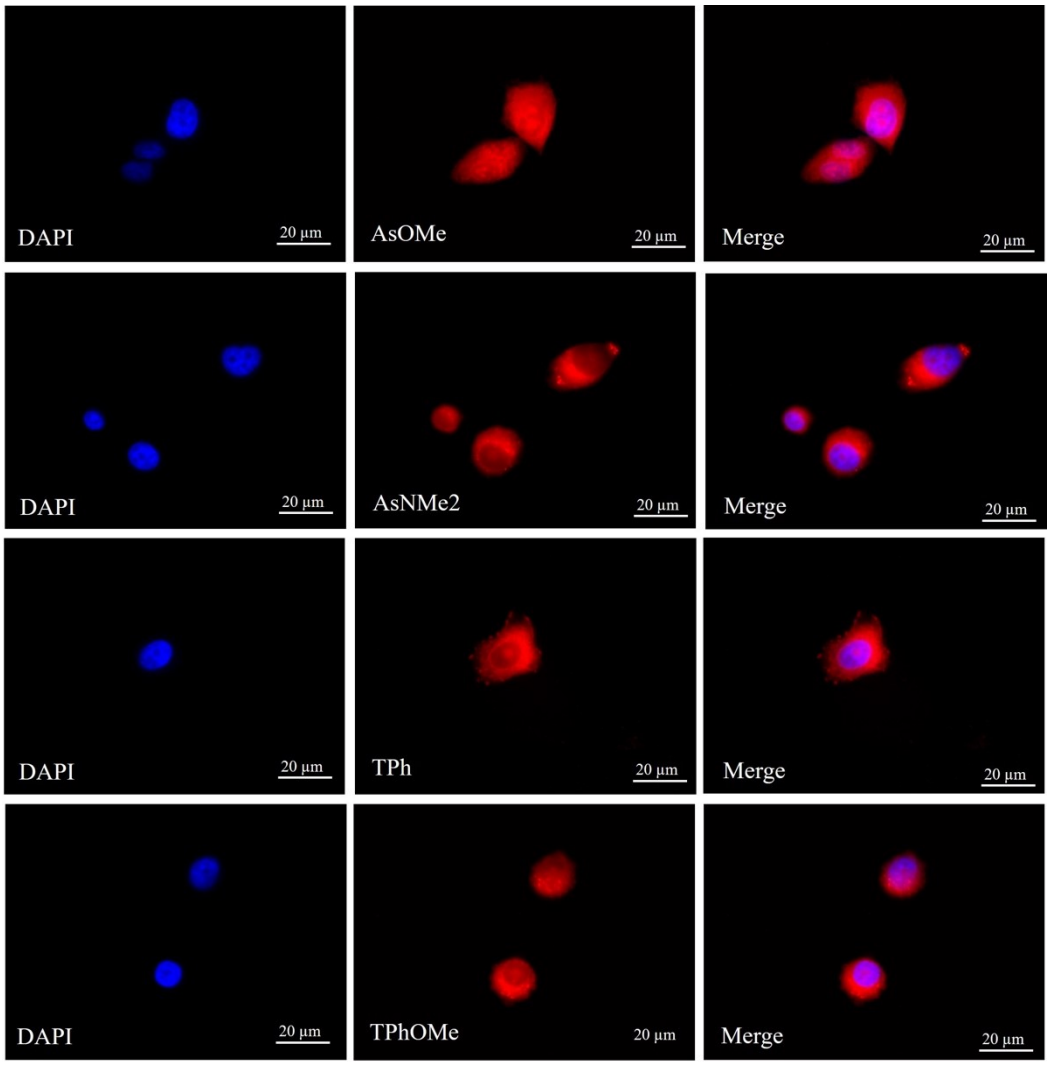

Figure S59. Representative fluorescence microscopy images of fixed LN-CaP cells. Cells stained with DAPI (blue, DAPI filter) and 10 µM pAQM compounds (red, TRITC filter) and merged images (image magnification: 60×).

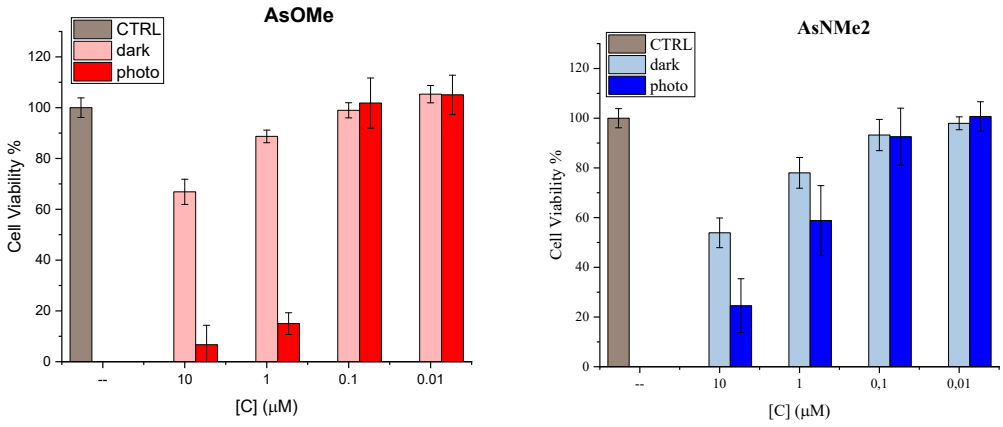

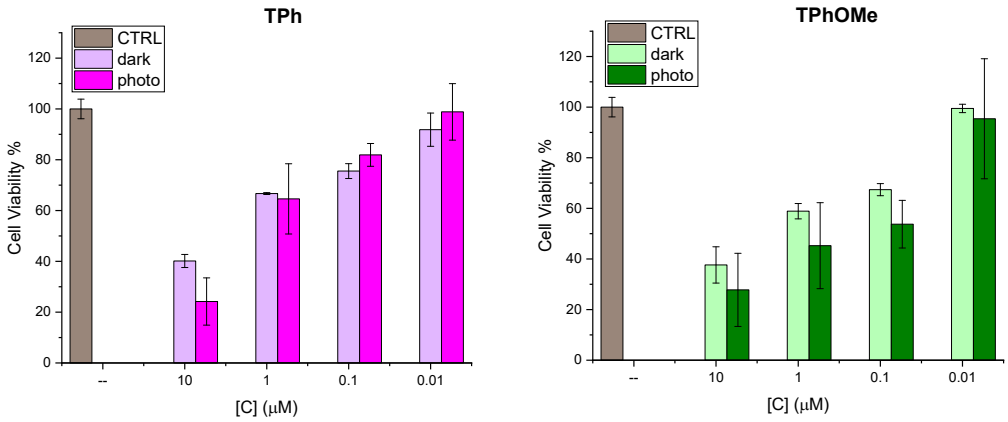

Figure S60. Dark cytotoxicity and Phototoxicity of the pAQM compounds on LN-CaP cells with a 28-minute irradiation time (corresponding to 1.80 J/cm^2). Both dark citotoxicity and phototoxicity are expressed as the mean of two independent experiments of four replicas each ± SD. 100% corresponds to the control mean values.

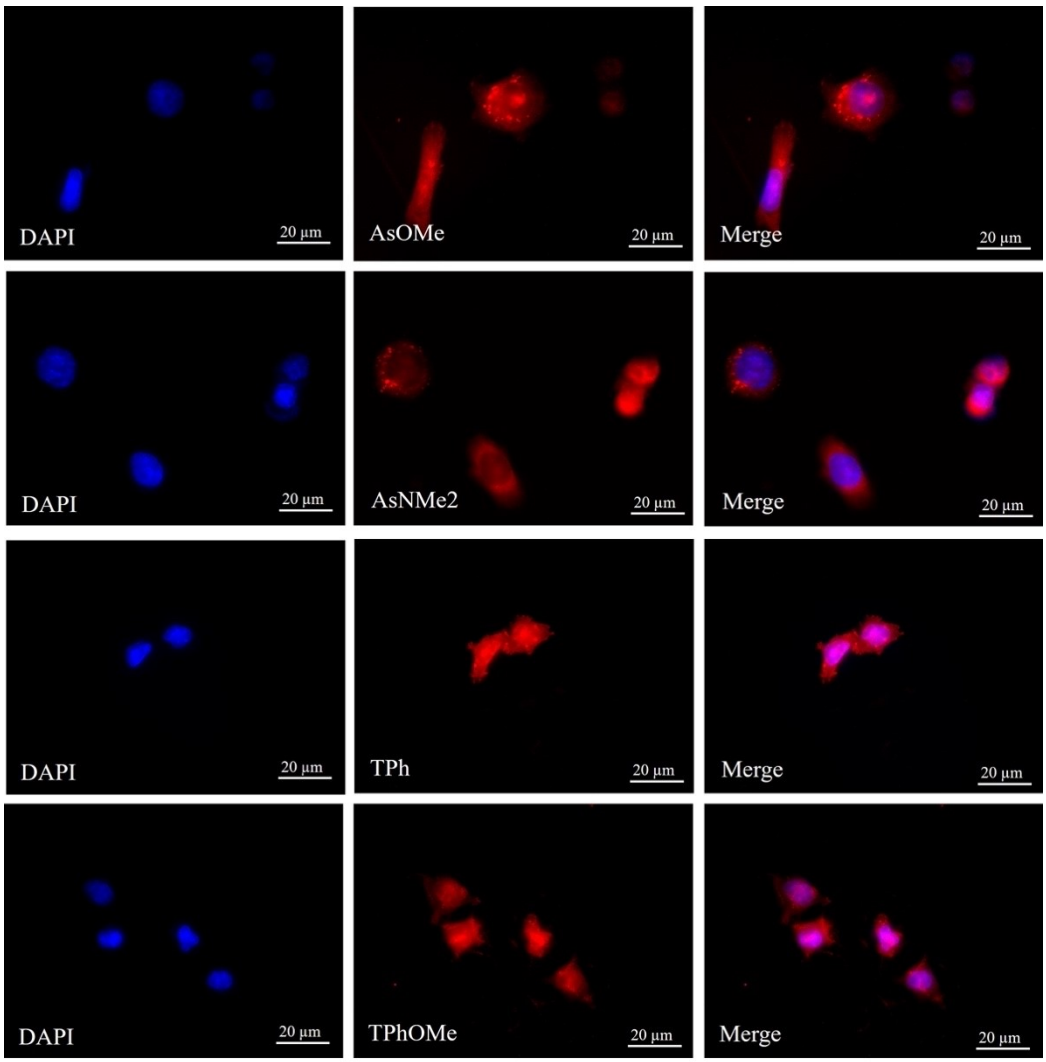

Figure S61. Representative fluorescence microscopy images of fixed Mel-501 cells. Cells stained with DAPI (blue, DAPI filter) and 10 μM pAQM compounds (red, TRITC filter) and merged images (image magnification: 60×).

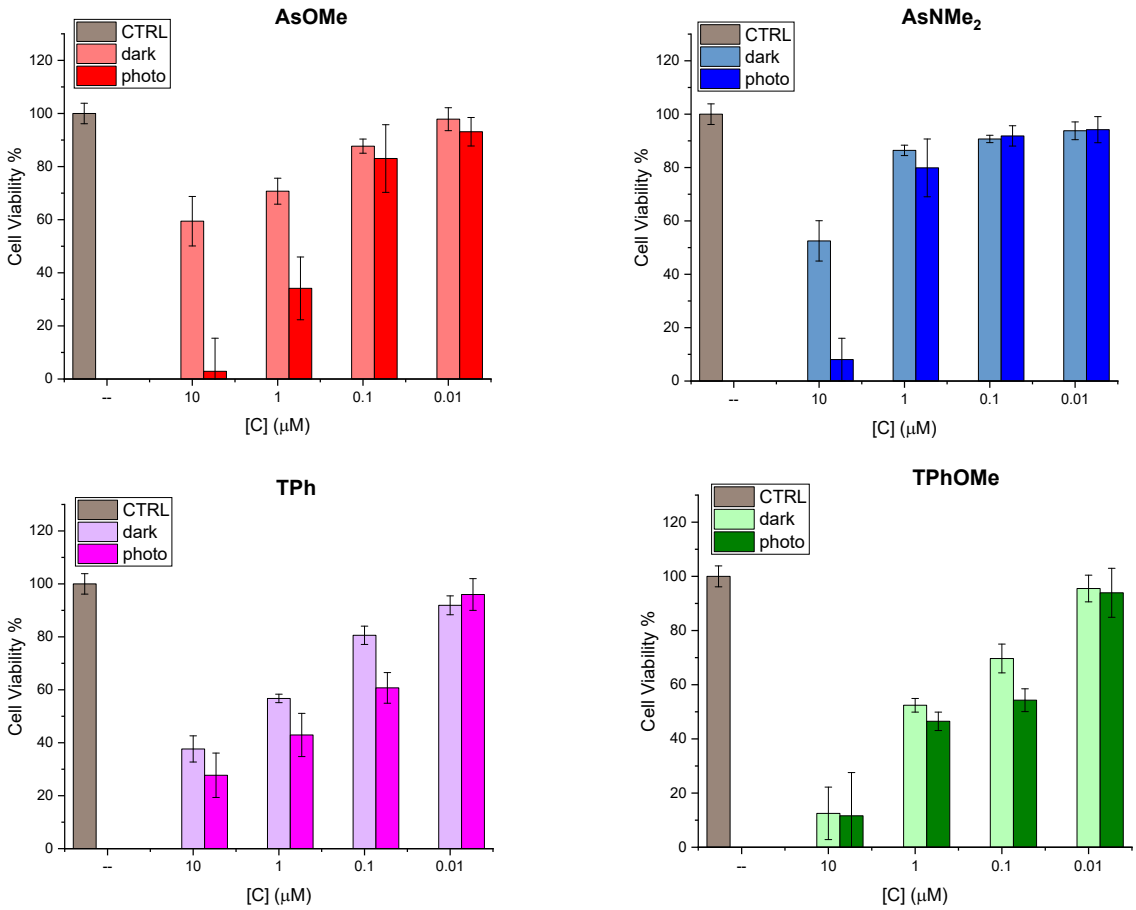

Figure S62. Dark cytotoxicity and Phototoxicity of the pAQM compounds on Mel-501cells with 28 minutes irradiation time (corresponding to 1.80 J/cm^2). Both dark cytotoxicity and phototoxicity are expressed as the mean of two independent experiments of four replicas each ± SD. 100% corresponds to the control mean values.

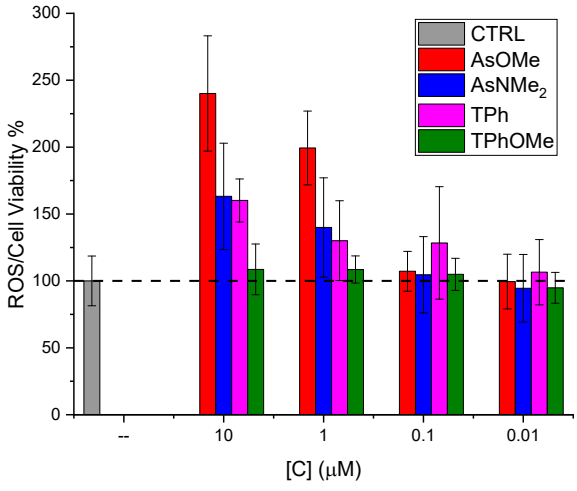

Figure S63. ROS production induced by the pAQM compounds on Mel-501 cells with 28 minutes irradiation time (1.80 J/cm^2). ROS production is expressed as mean of two independent experiments of four replicas each ± SD. 100% corresponds to the control mean values.

Fluorimetric ROS Tests

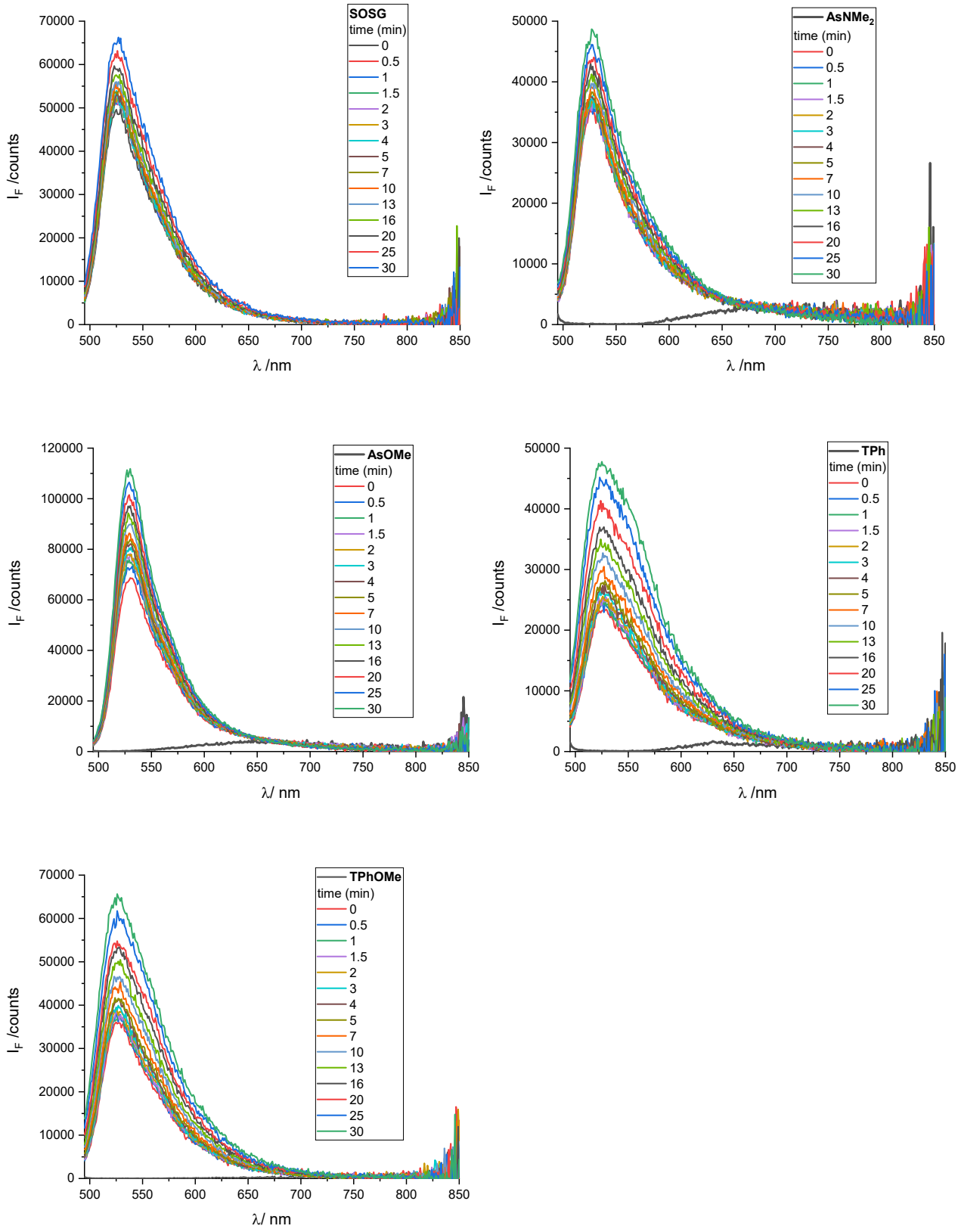

Figure S64. Emission spectra of the SOSG singlet oxygen probe (λ_{exc} = 488 nm) as a function of irradiation time under 458 nm light (1.07 mW/cm^2), alone as a control and in the presence of water-dispersed aggregates of the quinoidal compounds under investigation. Water-dispersed aggregates were produced by DMSO injection (2% v/v) into water upon probe sonication.

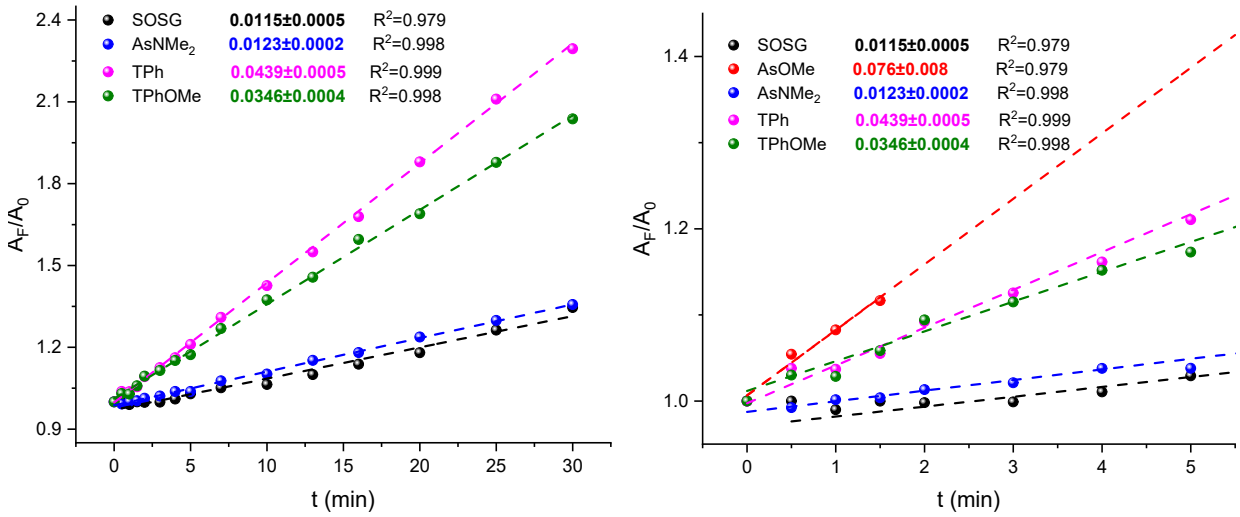

Figure S65. Area of the emission spectra of the SOSG singlet oxygen probe as a function of irradiation time under 458 nm light (1.07 mW/cm^2) for water-dispersed aggregates of the quinoidal compounds **(**produced by DMSO injection into water upon sonication) in the presence of SOSG and for the fluorescent probe alone as a control over a 30-minute irradiation time. Right graph: zoom in on the first 5 minutes of irradiation.

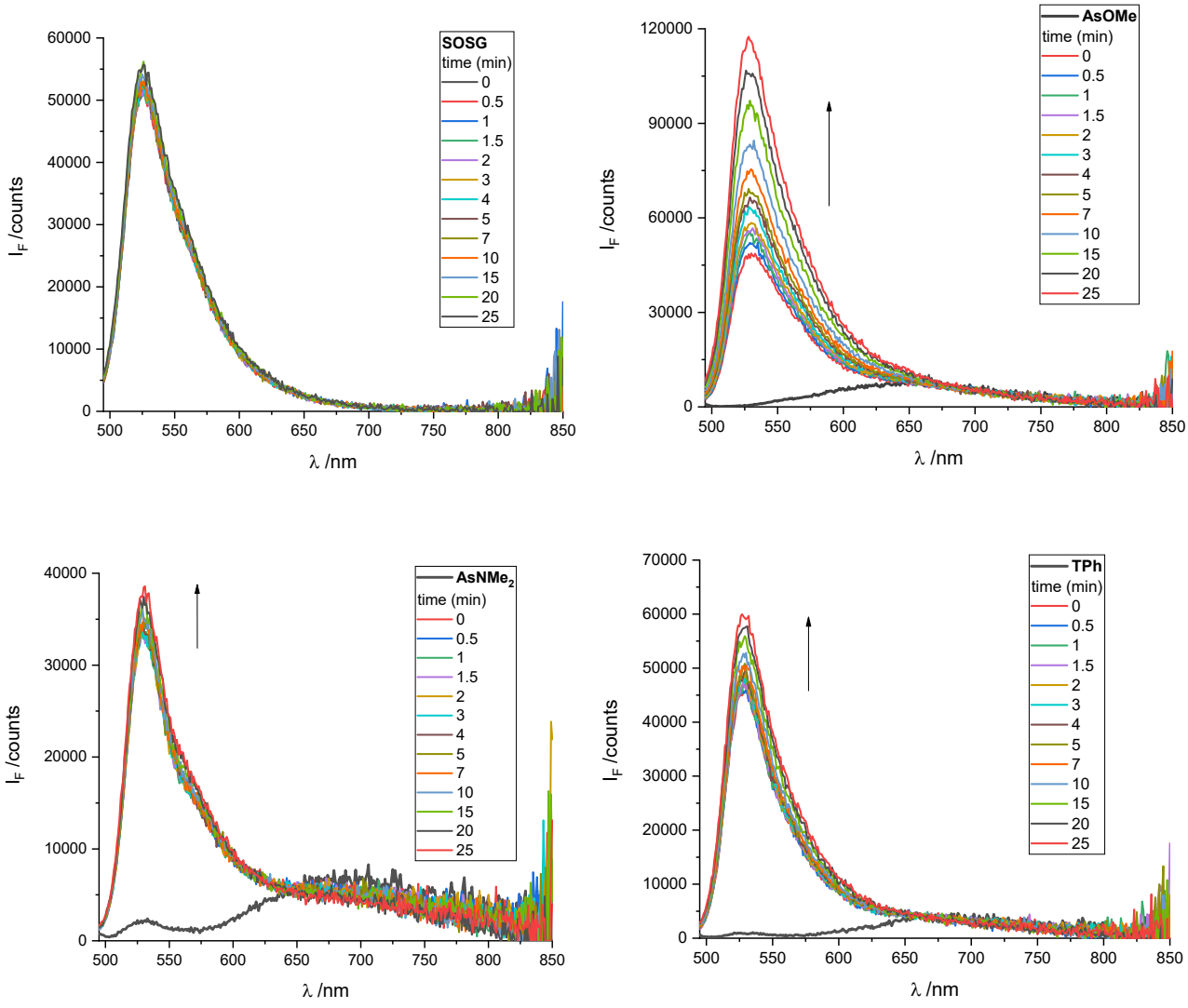

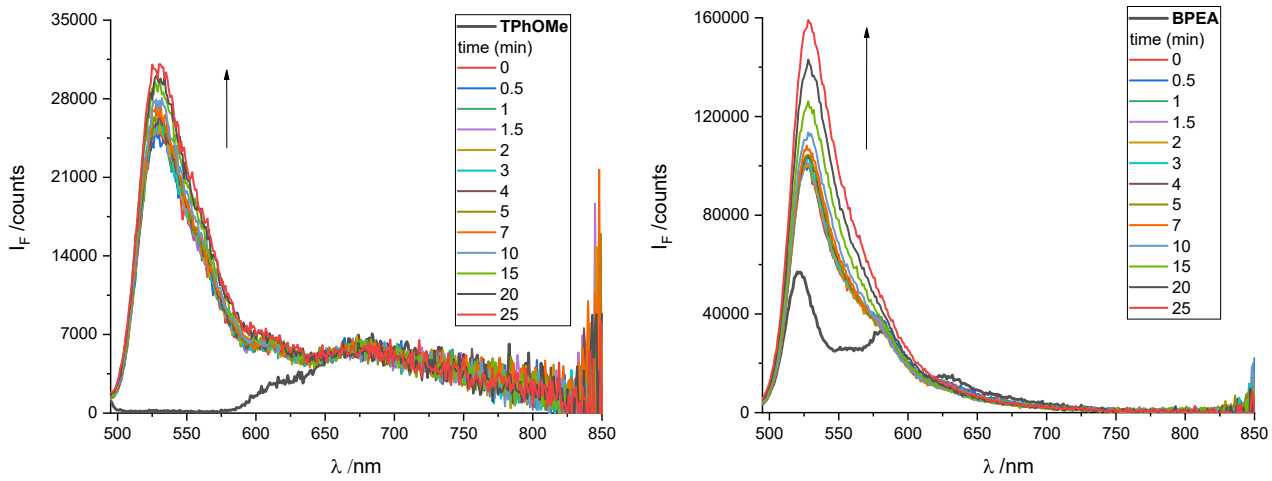

Figure S66. Emission spectra of the SOSG singlet oxygen probe (λ_{exc} = 488 nm) as a function of irradiation time under 458 nm light (1.07 mW/cm^2), alone as a control and in the presence of water-dispersed aggregates of either the quinoidal compounds under investigation or the reference compound BPEA. Water-dispersed aggregates were produced by THF injection (1% v/v) into water upon probe sonication.

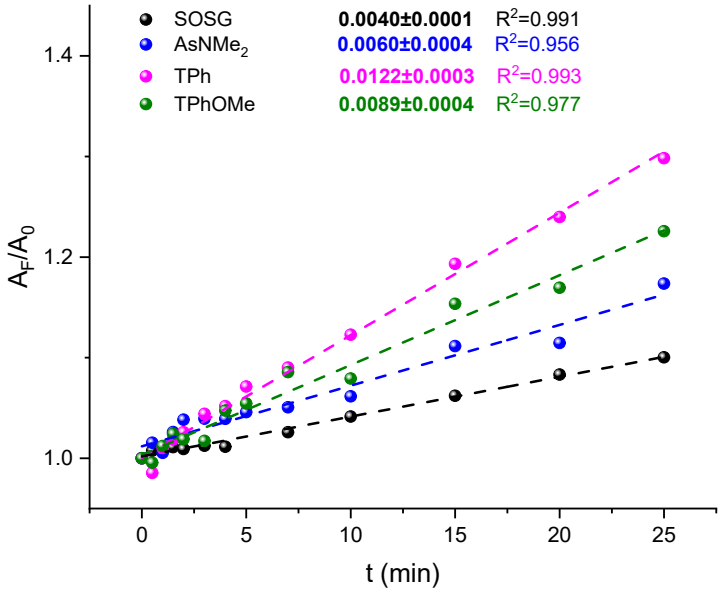

Figure S67. Area of the emission spectra of the SOSG singlet oxygen probe as a function of irradiation time under 458 nm light (1.07mW/cm^2) for water-dispersed aggregates of the quinoidal compounds (produced by THF injection into water upon sonication)in the presence of SOSG and for the fluorescent probe alone as a control over a 25-minute irradiation time.

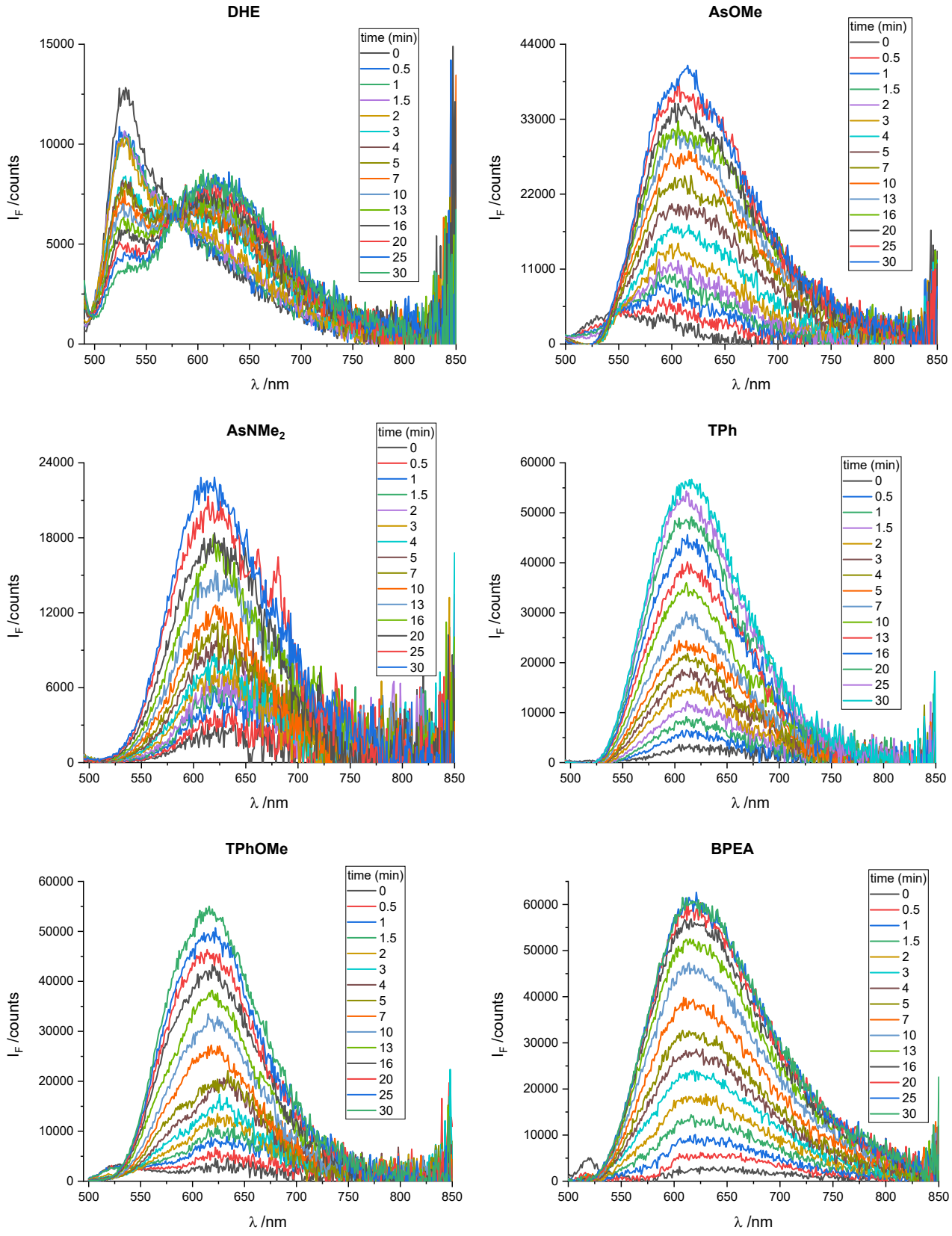

Figure S68. Emission spectra of the DHE superoxide anion probe (λ_{exc} = 480 nm) as a function of irradiation time under 458 nm light (1.07 mW/cm^2), alone as a control and in the presence of water-dispersed aggregates of either the quinoidal compounds under investigation or the reference compound BPEA. Water-dispersed aggregates were produced by THF injection (1% v/v) into water

upon probe sonication. Emission spectra are reported after subtraction of the contribution of the fluorescence of the water-dispersed aggregates.

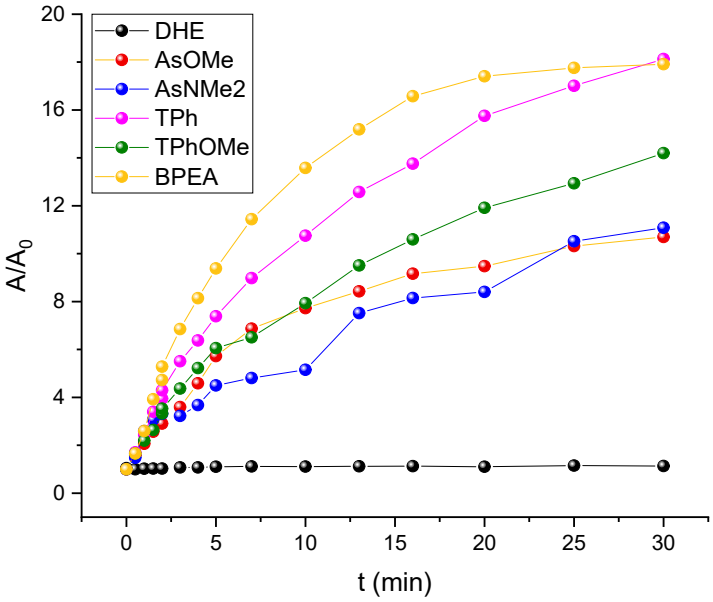

Figure S69. Area of the emission spectra of the DHE superoxide anion probe as a function of irradiation time under 458 nm light (1.07 mW/cm^2) for water-dispersed aggregates of the quinoidal compounds **(**produced by THF injection into water upon sonication) in the presence of DHE and for the fluorescent probe alone as a control over a 30-minute irradiation time.

(1) Alebardi, M.; Carella, A.; Grasso, A.; Sorbelli, E.; Lazzarin, F.; Munzone, C.; Fortuna, C. G.; Elisei, F.; Spalletti, A.; Bonaccorso, C.; Valentin, M. D.; Carlotti, B. Singlet Fission in Push–Pull Para-Azaquinodimethane Films under the Gaze of Time Resolved Optical and Magnetic Spectroscopy. *Angewandte Chemie International Editionn/a* (n/a), e20838. https://doi.org/10.1002/anie.202520838.

(2) Mancini, P.; Montanari, C.; Venturi, P.; Yadav, K.; Bianconi, T.; Calzoni, E.; Cesaretti, A.; Misra, R.; Carlotti, B. Tuning the Fate of the Triplet by Changing the Degree of Branching in Phenothiazine–Trithienyltriazine Nanoaggregates. *Chemical Communications***2025**, *61* (99), 19628–19631. https://doi.org/10.1039/D5CC05041C.

(3) Cantoni, R.; Alebardi, M.; D'Amato, E. M.; Popli, C.; Patil, Y.; Mancini, P.; Di Michele, A.; Spalletti, A.; Misra, R.; Goodson, T.; Carlotti, B. Unveiling Aggregation-Induced Singlet Fission in Push–Pull Diketopyrrolopyrrole Water Dispersed Nanoaggregates and Thin Films. *Advanced Functional Materialsn/a* (n/a), e17911. https://doi.org/10.1002/adfm.202517911.

(4) Montalti, M.; Credi, A.; Prodi, L.; Gandolfi, M. T. *Handbook of Photochemistry*, 3rd ed.; CRC Press: Boca Raton, 2006. https://doi.org/10.1201/9781420015195.

(5) Carmichael, I.; Hug, G. L. Triplet–Triplet Absorption Spectra of Organic Molecules in Condensed Phases. *Journal of Physical and Chemical Reference Data***1986**, *15* (1), 1–250. https://doi.org/10.1063/1.555770.

(6) Mencaroni, L.; Carlotti, B.; Elisei, F.; Marrocchi, A.; Spalletti, A. Exploring a New Class of Singlet Fission Fluorene Derivatives with High-Energy Triplets. *Chem. Sci.***2022**, *13* (7), 2071–2078. https://doi.org/10.1039/D1SC07175K.

(7) Ricci, F.; Elisei, F.; Foggi, P.; Marrocchi, A.; Spalletti, A.; Carlotti, B. Photobehavior and Nonlinear Optical Properties of Push–Pull, Symmetrical, and Highly Fluorescent Benzothiadiazole Derivatives. *J. Phys. Chem. C***2016**, *120* (41), 23726–23739. https://doi.org/10.1021/acs.jpcc.6b07290.

(8) Xu, C.; Webb, W. W. Measurement of Two-Photon Excitation Cross Sections of Molecular Fluorophores with Data from 690 to 1050 Nm. *J. Opt. Soc. Am. B***1996**, *13* (3), 481. https://doi.org/10.1364/JOSAB.13.000481.

(9) Lin, H.; Shen, Y.; Chen, D.; Lin, L.; Wilson, B. C.; Li, B.; Xie, S. Feasibility Study on Quantitative Measurements of Singlet Oxygen Generation Using Singlet Oxygen Sensor Green. *J Fluoresc***2013**, *23* (1), 41–47. https://doi.org/10.1007/s10895-012-1114-5.

(10) Nazarewicz, R. R.; Bikineyeva, A.; Dikalov, S. I. Rapid and Specific Measurements of Superoxide Using Fluorescence Spectroscopy. *J Biomol Screen***2013**, *18* (4), 498–503. https://doi.org/10.1177/1087057112468765.

(11) Bresolí-Obach, R.; Busto-Moner, L.; Muller, C.; Reina, M.; Nonell, S. NanoDCFH-DA: A Silica-Based Nanostructured Fluorogenic Probe for the Detection of Reactive Oxygen Species. *Photochemistry and Photobiology***2018**, *94* (6), 1143–1150. https://doi.org/10.1111/php.13020.

(12) Margulies, E. A.; Miller, C. E.; Wu, Y.; Ma, L.; Schatz, G. C.; Young, R. M.; Wasielewski, M. R. Enabling Singlet Fission by Controlling Intramolecular Charge Transfer in π-Stacked Covalent Terrylenediimide Dimers. *Nature Chem***2016**, *8* (12), 1120–1125. https://doi.org/10.1038/nchem.2589.

(13) Carlotti, B.; Madu, I. K.; Kim, H.; Cai, Zhengxu.; Jiang, H.; Muthike, A. K.; Yu, L.; Zimmerman, P. M.; Goodson, T. Activating Intramolecular Singlet Exciton Fission by Altering π-Bridge Flexibility in Perylene Diimide Trimers for Organic Solar Cells. *Chem. Sci.***2020**, *11* (33), 8757–8770. https://doi.org/10.1039/D0SC03271A.